frontiers | Frontiers in Earth Science

TYPE Original Research
PUBLISHED 23 September 2024
DOI 10.3389/feart.2024.1464924

OPEN ACCESS

EDITED BY
Yosuke Aoki,
The University of Tokyo, Japan

REVIEWED BY
Qiang Li,
China University of Petroleum Beijing, China
Majid Khan,
University of Science and Technology Beijing, China

*CORRESPONDENCE
Ruizhao Yang,
yrz@cumtb.edu.cn

RECEIVED 15 July 2024
ACCEPTED 03 September 2024
PUBLISHED 23 September 2024

CITATION
Guo J, Yang R, Geng F, Wang L, Zhang S, Wang L and Han F (2024) Segmentation characteristics of strike-slip fault zone and its reservoir control mechanisms in the southwestern Tarim Basin.
Front. Earth Sci. 12:1464924.
doi: 10.3389/feart.2024.1464924

Segmentation characteristics of strike-slip fault zone and its reservoir control mechanisms in the southwestern Tarim Basin

Jialiang Guo[1], Ruizhao Yang[1]*, Feng Geng[2], Li Wang[3], Shijie Zhang[1], Lingda Wang[1] and Fengtao Han[1]

[1]College of Geoscience and Surveying Engineering, China University of Mining and Technology, Beijing, China, [2]Petroleum Exploration and Production Research Institute of Northwest Oilfield Company Sinopec, Urumqi, China, [3]Sinopec Petroleum Exploration and Production Research Institute, Beijing, China

Understanding how fault-related structures influence oil and gas accumulation is crucial for geological investigations and exploration planning. This study, based on 3D seismic data, analyzes the northeast-trending strike-slip fault zone in the eastern part of the Bachu Uplift. Automatic fault extraction techniques were employed to delineate the strike-slip fault zone, and the parallel bedding indicator was used to identify reservoirs and investigate the fault's segmented features and reservoir-controlling characteristics. The results show that the northeast-trending strike-slip fault is primarily governed by simple shear stress and conforms to the Riedel shear model. Three distinct structural styles were developed: vertical, pull-apart, and push-up segments, each exhibiting varying profile characteristics and planar patterns. The segmentation of the strike-slip fault controls the distribution of Ordovician fault-karst reservoirs. An oil and gas enrichment model for the strike-slip fault zone has been established, characterized by external hydrocarbon supply, fault-mediated migration, segmented reservoir control, and high-elevation accumulation. This study offers valuable insights for the exploration of fault-karst reservoirs controlled by strike-slip faults.

KEYWORDS

strike-slip faults, fault-karst reservoirs, segmentation, structure characterization, Tarim Basin

1 Introduction

The structural segmentation of strike-slip faults is a common geological phenomenon (Wu et al., 2016). The geometric characteristics of fault segmentation have been extensively studied (Benesh et al., 2014; Carne and Little, 2012; Kumar et al., 2023; Li et al., 2023; Sylvester, 1988; Woodcock and Fischer, 1986), and their impact on reservoirs in hydrocarbon-bearing basins has also been well-documented (Brister et al., 2002; Cui et al., 2022; He et al., 2023; Liang et al., 2020; Rotevatn and Bastesen, 2014). These studies indicate that fault segmentation plays a crucial role in the structural analysis of fault zones and in the prediction of fault-controlled reservoirs.

The primary focus of exploration in the Tarim Basin is based on the Ordovician carbonate fault-karst reservoirs, wherein strike-slip faults are crucial

in reservoir composition and hydrocarbon accumulation (Han et al., 2017). These deep-seated strike-slip faults, many of which extend into the basement, serve as effective conduits for vertical oil and gas migration. Simultaneously, they can alter carbonate reservoirs, significantly enhancing their properties (Zhao et al., 2023). Elaborating on this foundation, some studies have introduced the novel concept of "Fault-Karst Carbonate Reservoirs" (Ding et al., 2020; Lu et al., 2017). Research on strike-slip faults has predominantly focused on exploring structural patterns (Li et al., 2013; Lv et al., 2022; Qi, 2021), development, and evolution (Chemenda et al., 2016; Xiao et al., 2017), as well as their impact on the modification of carbonate reservoirs and the control of oil and gas traps (Lu et al., 2016; Lv et al., 2022; Qi, 2021; Ramadhan et al., 2018; Sun et al., 2023; Wang et al., 2020; Wang et al., 2021; Wang et al., 2023).

The Ordovician strike-slip faults in various blocks of the Tarim Basin exhibit considerable variation in their formation mechanisms (Chen et al., 2022; Jia et al., 2022; Wu et al., 2021). However, they are similar regarding profile patterns and planar distribution characteristics. For example, these features frequently exhibit segmented characteristics in plan view and flower structures when examined in profile (Han et al., 2017). These characteristics play a significant role in controlling oil and gas accumulation. According to Qi (2021), the Shun one strike-slip fault zone in the Shunbei area can be classified into three types: vertical, pull-apart, and compressive, comprising nine fault segments. The characteristics of each segment influence the scale and quality of reservoir development, with oil and gas accumulating and forming reservoirs along flower-shaped or upright structural fault surfaces. Wang et al. (2020) conducted a systematic study of the oil and gas characteristics of the SB1 fault by analyzing high-quality 3D seismic data, outcrop data, drilling data, and production information. They categorized the SB1 fault into linear shear structural segments without deformation, pull-apart structural segments, and uplifted structural segments. Their findings indicated that pull-apart structural segments are the most favorable regions for oil and gas accumulation. Deng et al. (2019) conducted a segmentation study of strike-slip faults in the central Tarim Basin based on the vertical variations in the fault. Lv et al. (2022) conducted a study on the segmentation of the TP12CX strike-slip fault. They combined the drilling and production data to demonstrate that different fault segments exhibit varying reservoir configurations and hydrocarbon potentials. They classified four types of strike-slip fault segments and their corresponding reservoir models. Zhang et al. (2021) provided a detailed description of the segmental deformation characteristics and reservoir-controlling features of the S-1, S-7, and S-5M fault zones based on seismic, well logging, and core data. However, there is still a lack of an oil and gas enrichment model related to the segmentation of strike-slip faults to guide exploration and development. Therefore, it is particularly important to strengthen the characterization and evaluation of the strike-slip fault zone and its associated reservoirs.

Before this, the primary task is to enhance the interpretation of strike-slip faults. Manual interpretation of complex strike-slip faults is time-consuming and labor-intensive, and it can also increase uncertainty. It is well known that 3D seismic data has high resolution, which can be used to extract various seismic attributes to reveal more details of faults (Chopra and Marfurt, 2007; Frankowicz and McClay, 2010; Gui et al., 2021; Yao et al., 2024). In this study, using the Bachu Uplift in the southwestern Tarim Basin as a case study, frequency decomposition preprocessing on 3D seismic data was first conducted to enhance the discontinuities of strike-slip fault zone, followed by segmentation interpretation of the fault based on seismic attributes. The relationship between the segmented strike-slip fault zone and reservoirs was examined with regard to aspects such as map view patterns and profile characteristics. This study aims to provide fresh perspectives for the exploration of deep strike-slip fault-controlled carbonate reservoirs and oil and gas development in the Tarim Basin or similar regions.

This study has the following highlights: First, a fault-karst reservoir prediction method based on Parallel Bedding Indicator attribute is proposed, using seismic amplitude as input to emphasize the seismic response of such reservoirs, which can serve as a reference for predicting carbonate fault-karst reservoirs. Second, it is demonstrated that strike-slip faults in the southwestern Tarim Basin conform to the Riedel structural model, exhibiting distinct segmentation in the map view. Third, a segmented oil and gas accumulation model controlled by strike-slip fault zone in carbonate rocks is established, offering new insights for oil and gas exploration in similar regions.

2 Geological setting

2.1 Geological overview

The Tarim Basin is located in northwestern China (Figure 1A). Covering a vast area of 56×10^4 km^2, it is the largest oil and gas basin in China. Multiple combinations of sources, reservoirs, and cap rocks exist within this basin, resulting in an abundance of oil and gas resources. The geological formations are diverse, with numerous oil- and gas-bearing strata characterized by excellent reservoir properties and favorable conditions for hydrocarbon accumulation (Jia and Wei, 2002). It can be divided into seven first-order tectonic units (He and Zheng, 2016). The Ordovician carbonate reservoirs in the Tarim Basin have yielded a total oil and gas volume exceeding 1.6 billion tons of oil equivalent for more than 50 years of exploration, establishing the Ordovician system as a significant oil- and gas-bearing system within the basin (Pang et al., 2010).

The Bachu Uplift, located in the southwestern region of the Tarim Basin, spans an area of 47,500 km^2 (Yu et al., 2010). This region constitutes a secondary structural unit in the Tarim Basin (Figure 1B). Generally, the Bachu Uplift features a northwest-high and southeast-low configuration, resembling a substantial nasal uplift. It predominantly extends in a northwesterly direction, with its eastern segment extending in the north-northwesterly (NNW) direction, whereas the western segment gradually extends in a northwesterly (NNW) direction (Tong et al., 2012). The target area of this study is located in the northern part of the Hetianhe Gas Field in the eastern segment of the Bachu Uplift (Figure 1C).

The eastern segment of the Bachu Uplift contains a stratigraphic sequence that encompasses the Neoproterozoic Sinian, Paleozoic Cambrian, Ordovician, Silurian, Devonian, Carboniferous, Permian, Mesozoic Triassic, Cretaceous, Cenozoic Neogene, and Quaternary. The overall stratigraphic sequence can be summarized as follows: Cambrian and Ordovician strata are widely distributed

10.3389/feart.2024.1464924

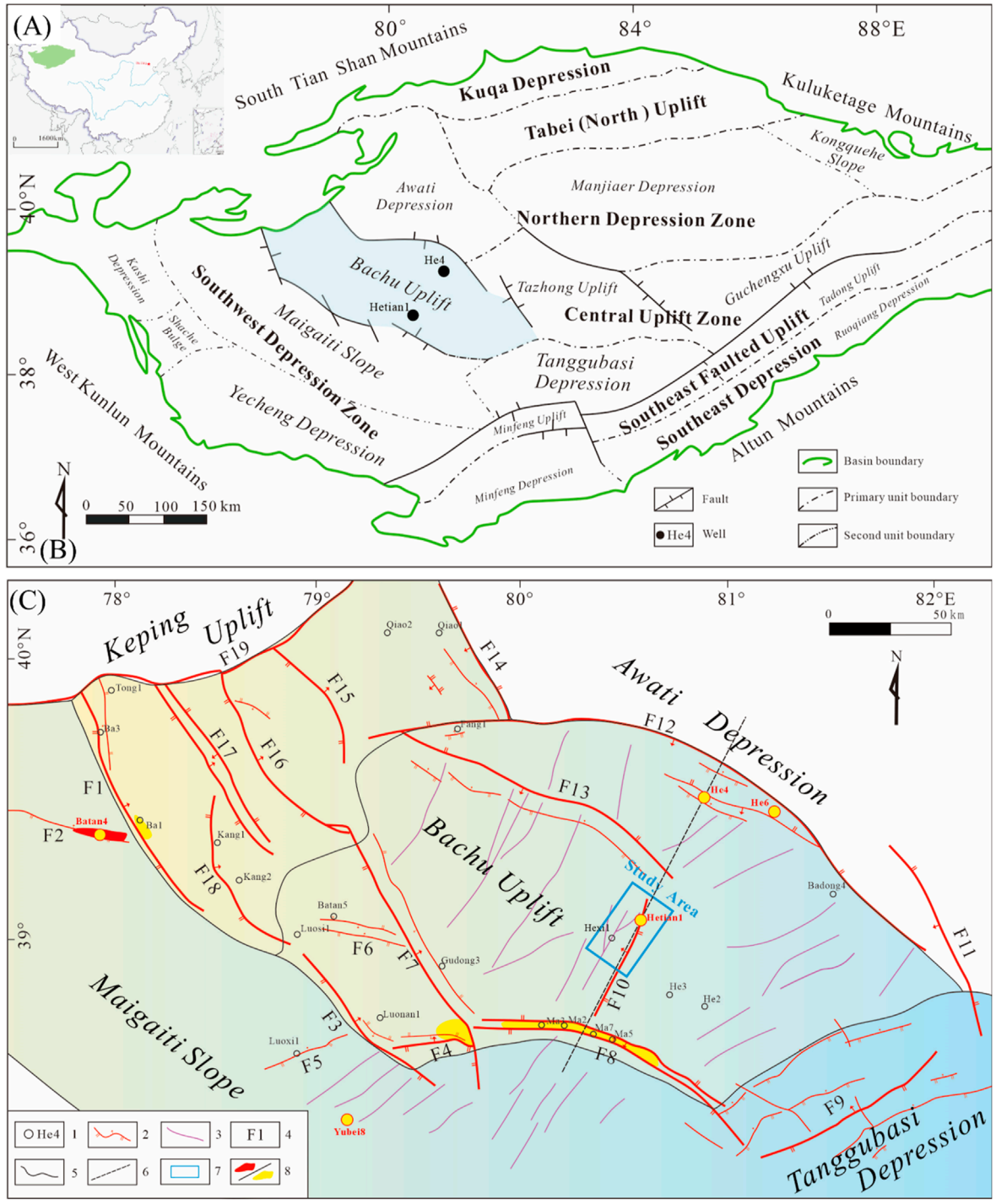

FIGURE 1
Structural units of Tarim Basin in northwestern China and plane map of the fault system of the Bachu Uplift **(A)**. The location of Taim basin in China **(B)**. Structural units of Tarim Basin **(C)**. Plane map of the fault system of the Bachu Uplift). Plane map of fault system of Bachu Uplift: 1. Well location; 2. Thrust fault; 3. Strike-slip fault; 4. Fault or fault belt number, F1. Selikbuya fault belt, F2. Bashituo fault, F3. Haimiluosi fault, F4. Niaoshan fault belt, F5. Luosi fault, F6. Haimidong fault belt, F7. Guodongshan fault belt, F8. Mazhatage Fault belt, F9. Madong fault belt, F10. Hetianhe five fault belt, F11. Badong fault, F12. Tumuxiuke fault belt, F13. Kalashayi fault belt, F14. Aqia-Piqiakexun fault belt, F15. Bielitage fault, F16. Bachu fault belt, F17. Qiaoxiaorgai fault belt, F18. Kangtakumu fault, F19. Keping fault; 5. Boundaries of tectonic units: 6. Profile; 7. Study area; 8. Oil and gas reservoir.

in the entire area, and the overall thickness remains relatively stable. Some Silurian and Devonian strata have been subjected to erosion. Carboniferous and Permian strata are extensively developed throughout the region, with a relatively stable thickness. Jurassic and Cretaceous strata are absent, with only Triassic strata present among the Mesozoic formations. Cenozoic strata are extensively

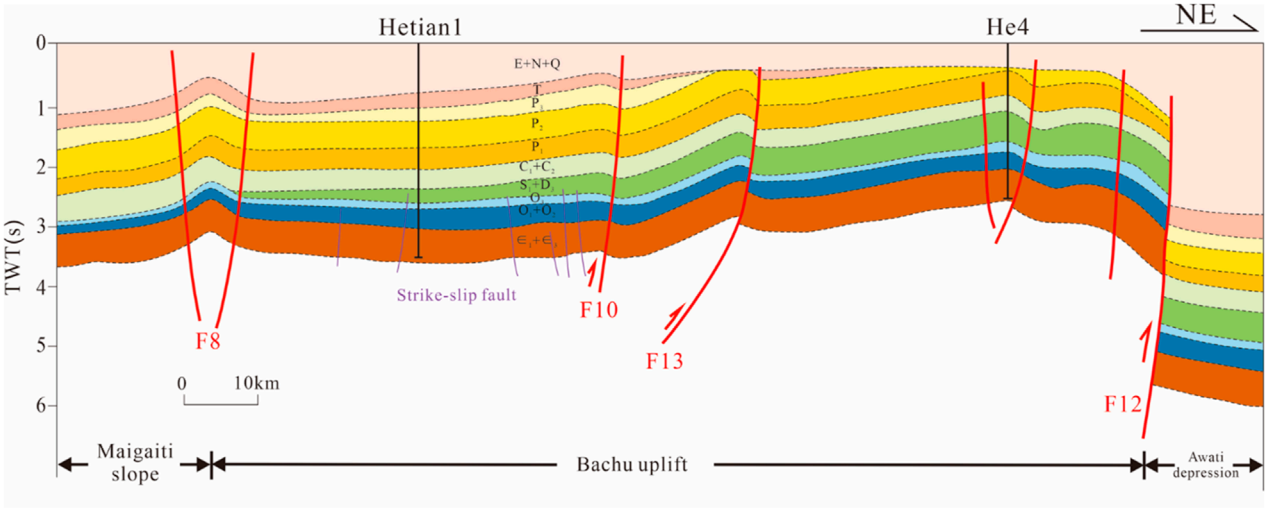

FIGURE 2
NE-SW trending stratigraphic profile across the middle Bachu Uplift (fault belt number and the profile location see Figure 1).

developed with stable thickness and have generally not been eroded. Overall, the northern region has experienced uplift influenced by the Tumuxiuke and Kalashayi fault belts, resulting in strong erosion. The strata in the interior of the uplift are relatively flat, as shown in Figure 2.

The target strata of this study are the Ordovician formations (Figure 3). The Penglaiba Formation, with seismic wave group T_8^0 marking its top, consists of thick layers of dark gray dolomite. The Yingshan Formation, with seismic wave group T_7^4 at its top, is composed of dark gray limestone, dolomite, and gray clastic limestone. The Lianglitage Formation, with seismic wave group T_7^2 at its top, is characterized by mudstone. The Sangtamu Formation, with seismic wave group T_7^0 at its top, consists of thick layers of calcareous mudstone (He et al., 2007; Song et al., 2021; Wang et al., 2021).

The Bachu Uplift, a secondary structural unit within the Tarim Basin, has experienced multiple significant tectonic events and superimposed evolutionary histories. It has generated a complex hydrocarbon accumulation process characterized by multi-source rock hydrocarbon generation, multi-stage accumulation, and mixed adjustments (Li et al., 2018). Vertically, it features multiple sets of source, reservoir, and cap-rock combinations, as shown in Figure 3 (Jia and Wei, 2002; Li et al., 2019; Li et al., 2021; Shen et al., 2019; You et al., 2018). The main reservoir types, from bottom to top, include: (1) Cambrian dolostone reservoirs, (2) Middle–Upper Ordovician clastic limestone reservoirs, (3) Silurian clastic rock reservoir, (4) Devonian clastic reservoir, and (5) Carboniferous-Permian carbonate rock reservoirs. Additionally, the region features four sets of regional cap rocks, primarily composed of gypsum and clastic sedimentary rocks. The Ordovician carbonate reservoirs in the Bachu Uplift were primarily shaped by dissolution processes, creating reservoirs of varying sizes, such as fractured vuggy and cave-type reservoirs (Ding et al., 2012). These reservoirs feature storage spaces primarily within dissolution pores, caves, fractures. In some instances, local Upper Ordovician mudstones create favorable cap-rock combinations with these reservoirs.

2.2 Evolution of the Bachu Uplift

The Bachu Uplift, through tectonic uplift and inversion during various significant geological periods, has undergone multiple tectonic events, including the Caledonian, Hercynian, Indosinian-Yanshan, and Himalayan orogenies, all occurring above the pre-Sinian basement (Jia et al., 1997; Kang and Kang, 1996). These events have ultimately shaped the present-day structural configuration of the region (Ding et al., 2012; Zhang et al., 2023).

Overall, its tectonic evolution can be divided into the following four stages: (1) the Caledonian tectonic stage (from the end of the Sinian to the end of the Late Devonian); (2) the Hercynian tectonic stage (Carboniferous to Permian); (3) the Indosinian to the Yanshan tectonic stage (Triassic to the end of the Jurassic); and (4) the Himalayan tectonic stage (end of the Paleogene to Neogene) (Ding et al., 2012; Zhang et al., 2023).

Caledonian Tectonic Stage: During the Precambrian to Early Ordovician period, under a localized extensional tectonic setting, the ancient continental plates began to rift and subside, marking the transition of the Tarim Basin into a craton-margin rift stage (Jia and Wei, 2002). During this time, the basin experienced extensive marine carbonate sedimentation (Kang and Kang, 1996), with the Bachu area situated in the central part of the southwestern Tarim craton depression. By the end of the Middle to Late Ordovician, the regional stress environment changed, leading to compression in the southern Tarim region. The Bachu Uplift was positioned at the forefront of this tectonic compression, resulting in significant erosion of the O_3 strata, with some areas showing complete absence. The exposed O_{1-2} strata were also subjected to erosion, leading to the formation of the T_7^4 unconformity (Zhang et al., 2021). From the Silurian to the Devonian, the Tarim Plate continued to experience strong compression from the Kunlun Plate. Both the southern and northern margins of the Tarim Basin were active continental margins, while the interior of the craton remained a depression, resulting in a series of littoral to shallow marine sedimentary deposits. During the Late

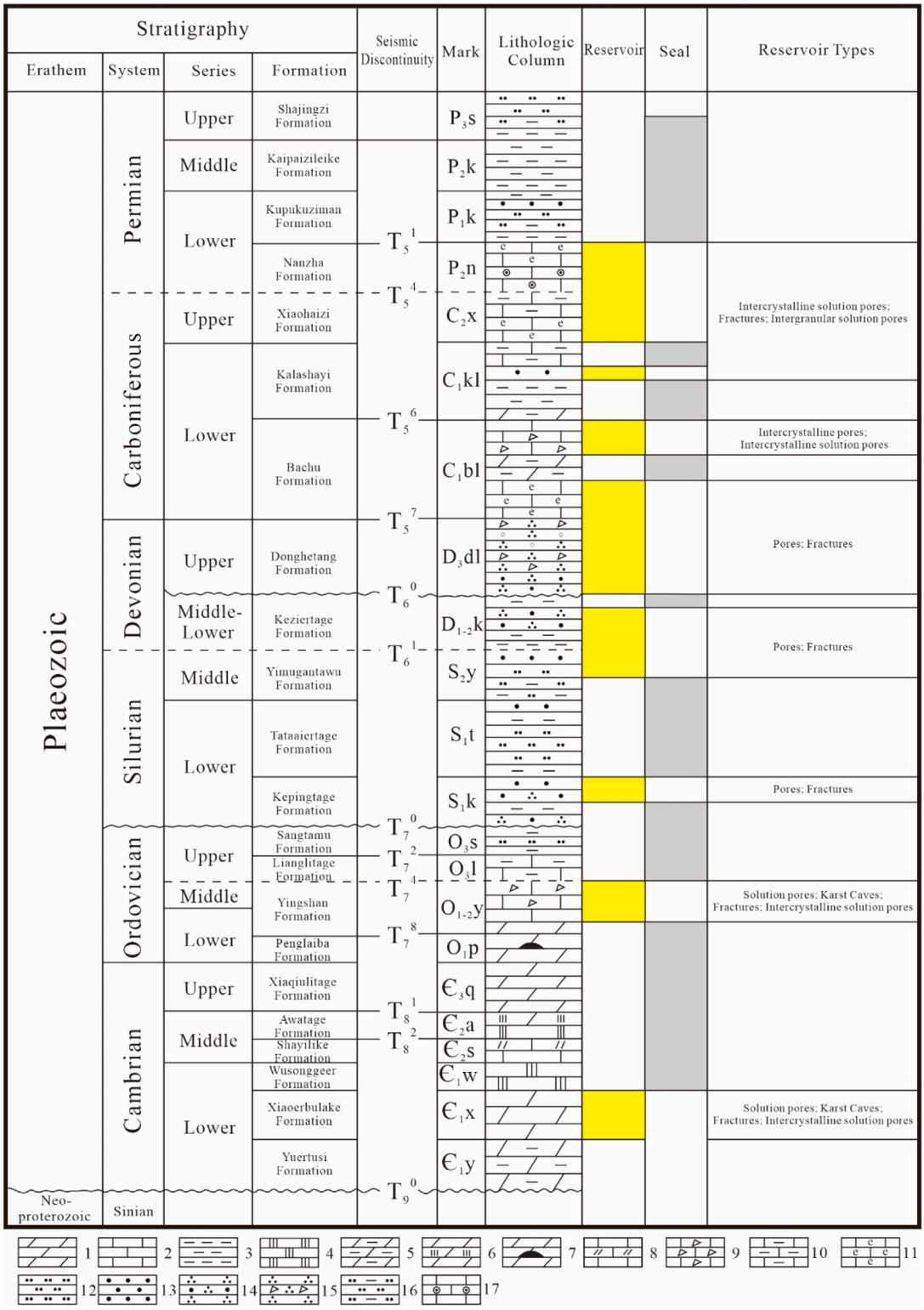

FIGURE 3
Paleozoic stratigraphic column of eastern Bachu Uplift. 1. Dolomite, 2. Limestone, 3. Mudstone, 4. Gypsum, 5. Argillaceous dolomite, 6. Gypsum dolomite, 7. Dolomite (containing flint nodules), 8. Dolomitic limestone, 9. Grained limestone, 10. Argillaceous limestone, 11. Bioclastic limestone, 12. Siltstone, 13. Fine sandstone, 14. Quartz sandstone, 15. Coarse-grained sandstone, 16. Silty mudstone, 17. Oolitic limestone. In the figure, numbers such as T_8^0 represent seismic discontinuity, sourced from (He et al., 2007; Song et al., 2021; Wang et al., 2021).

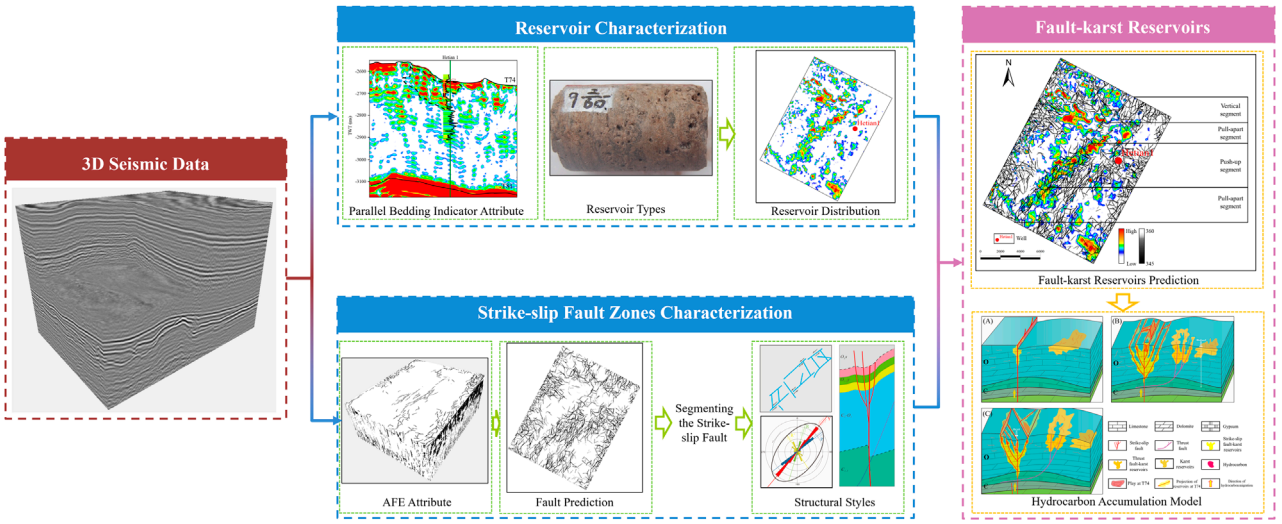

FIGURE 4
Research technical flowchart.

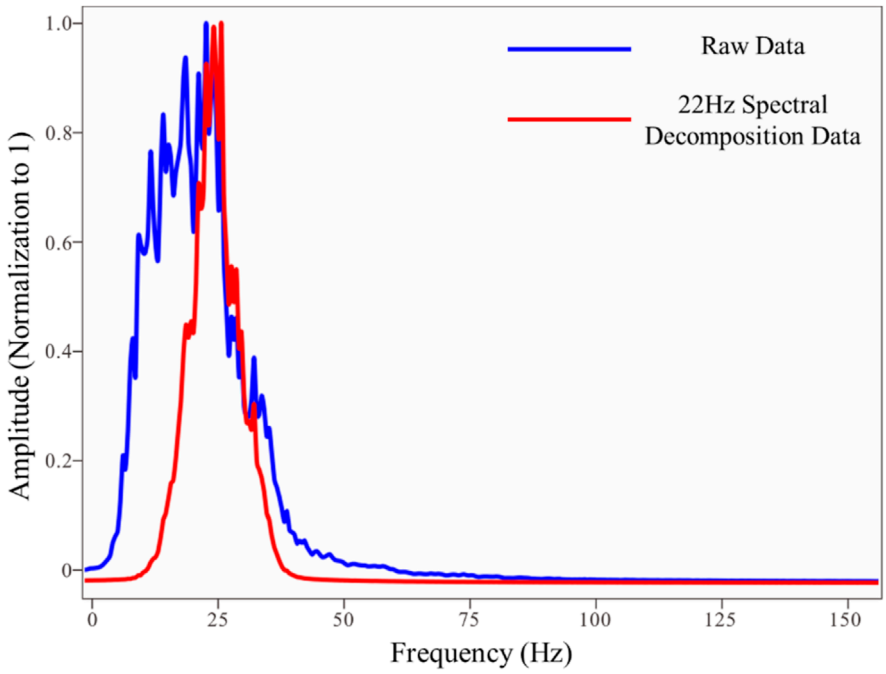

FIGURE 5
Spectrum calculation results. (The frequency band range of the decomposed data volume remained within the effective frequency band of the original seismic data).

Devonian, tectonic deformation intensified, with the development of a thrust belt in southern Tarim, accompanied by significant erosion (He et al., 2009; Jia and Wei, 2002), leading to the formation of the T_6^0 unconformity.

Hercynian Tectonic Stage: During the Carboniferous to Permian period, the Bachu Uplift experienced increased uplift, developing a slope feature between it and the southwestern Tarim depression. In the early Carboniferous, the Bachu area was characterized by an underwater uplift with stable subsidence and mixed sedimentation of clastic rocks and carbonates (Ding et al., 2008). The Carboniferous deposits are widely distributed in the Bachu area, with relatively uniform thickness (Lin et al., 2011; He et al., 2009). The Permian period saw frequent magmatic activity, leading to the development of mafic igneous rocks (Xiang et al., 2023).

Indosinian-Yanshan Tectonic Stage: At the end of the Triassic period, the collision between the Qiangtang block and the Tarim

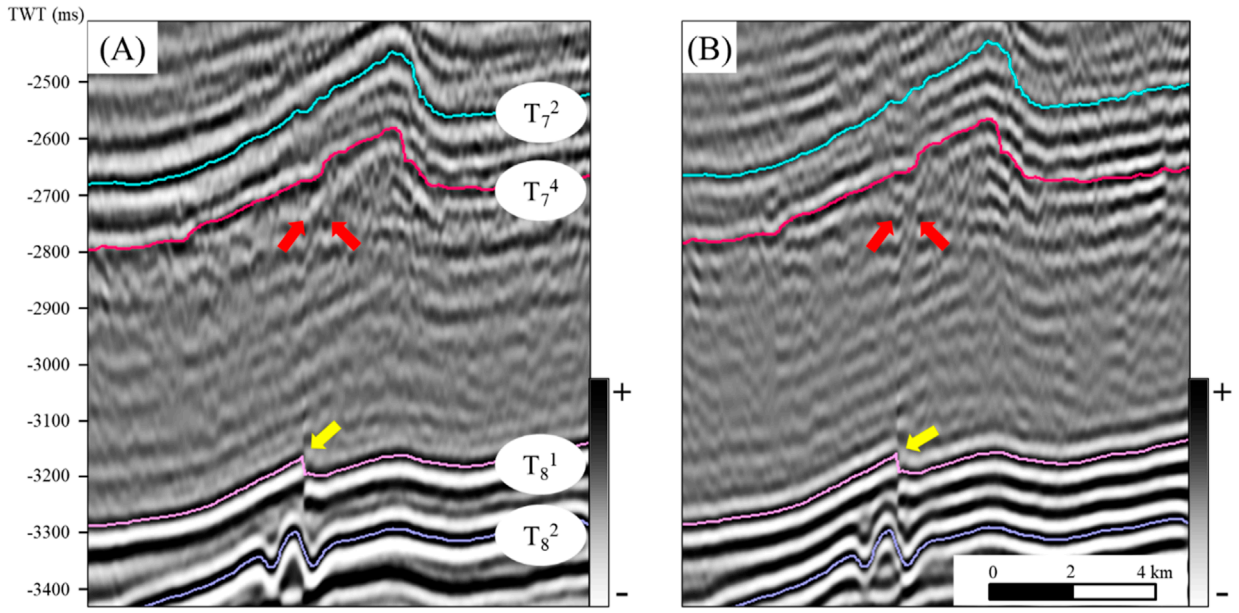

FIGURE 6
Comparison of cross-line 644 seismic sections **(A)** raw seismic section **(B)** 22 Hz seismic section (Compared with the original seismic data, the 22 Hz frequency-subdivided data volume exhibited the same fault segment characteristics along the base of the strike-slip fault zone (T_8^2) (indicated by yellow arrows); however, the flower structural features of the strike-slip fault zone at the top of the Yingshan Formation (T_7^4) (indicated by red arrows) were more pronounced).

Plate along the southern margin of the Tarim Basin caused further uplift of the surrounding orogenic belts, with the foreland depression located in front of the Kunlun Mountains (Ding et al., 2008). The Bachu Uplift continued to rise, with the Indosinian tectonic movement characterized by strong differential uplift and subsidence. The Bachu area became an erosion zone, a condition that persisted into the Yanshan period, resulting in the near-complete erosion of Mesozoic strata, corresponding to the T_5^0 tectonic unconformity.

Himalayan Tectonic Stage: At the end of the Paleogene, the Western Kunlun and Southern Tianshan orogenic belts thrust towards the Tarim Basin, leading to the folding, faulting, uplift, and erosion of the Bachu Uplift (Jia et al., 2004). During the Neogene period, the depressions on both sides of the Bachu Uplift experienced rapid subsidence, accompanied by intense activity along the boundary faults. The Miocene strata on the flanks of the uplift thinned and were eroded as they overstepped towards the uplift. After the Pliocene, the uplift continued its activity with diminishing tectonic forces, eventually reaching its present form.

The NE-trending strike-slip fault zone in the Bachu Uplift predominantly formed during the mid-Caledonian Stage I. During this period, the Bachu Uplift was subjected to a NE-oriented compressive stress field (Ding et al., 2008), leading to the development of several NE-trending strike-slip faults along pre-existing structural weakness zones. These fault zones continued to evolve and develop through subsequent tectonic events. They serve as conduits for fluid migration and play a constructive role in modifying carbonate reservoirs, which is conducive to the formation of interconnected large-scale fracture systems (Ding et al., 2020; You et al., 2018).

3 Data and methods

The 3D seismic data and well data from the study area and its vicinity were used in this study (well locations are indicated by yellow markers in Figure 1C). Besides, in the 3D seismic data, a total area of 406.9 km^2 and was in a full-stack configuration was coverd. The size of the 3D matrix was 701 × 931 × 4,600 (inline × crossline × time), and the inlines and crosslines were both spaced at 25 m. The time interval was 2 m. The 3D grid was laid out with inlines oriented NE-SW and crosslines running NW-SE, perpendicular to the inlines. The well data primarily consisted of log data and core photographs. Log curves were used to create composite well logs and calibrate seismic horizons, and core photographs were used to illustrate the reservoir types in the target layer (T_7^4).

Based on 3D seismic and well data, this study first applied spectral decomposition to seismic data to extract low-frequency information. Then, the faults were characterized using 3D seismic attributes, followed by a segmentation analysis of the faults based on seismic profiles. Subsequently, the Parallel Bedding Indicator attribute from the original seismic data was extracted to predict karst reservoirs. Finally, the fault interpretation results were combined with well data to propose a segmented hydrocarbon accumulation model controlled by the strike-slip fault zone in carbonate rocks. The technical workflow of this method is illustrated in Figure 4.

The specific methods of the study are listed as follows.

(1) Spectral decomposition preprocessing was applied to seismic data using a Continuous Wavelet Transform (CWT) based on the principles outlined by Sinha et al. (Sinha et al., 2005). Spectral decomposition technology provides clearer insights into fault features than conventional seismic profiling

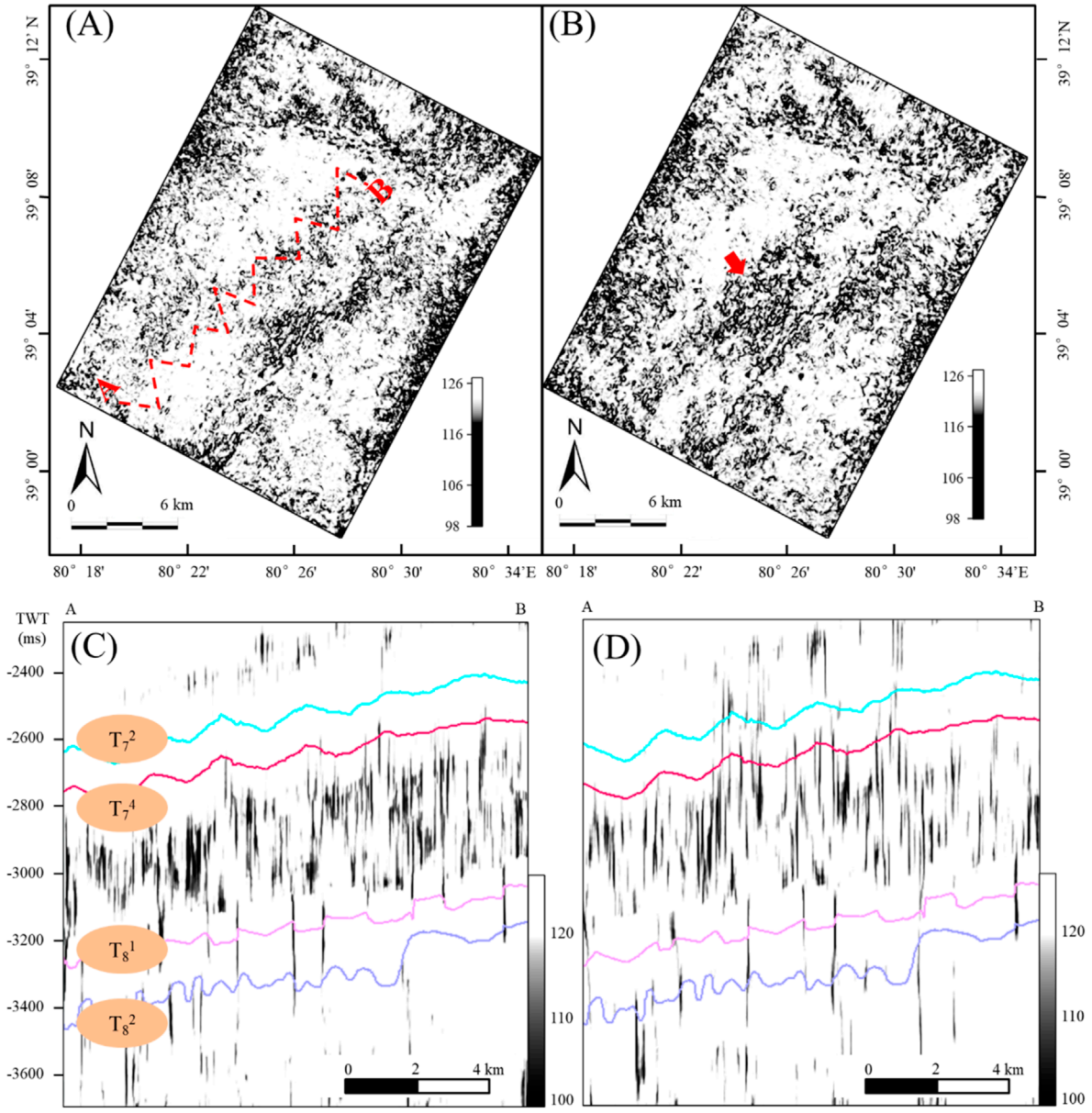

FIGURE 7
Coherent slices of T_7^4 and sections **(A)** raw seismic slice. **(B)** 22 Hz seismic slice. **(C)** raw and **(D)** 22 Hz seismic sections. (In **(A)**, the red dashed line AB indicates the profile locations for **(C, D)**. In **(B)**, the red arrows highlight the strike-slip fault zone as depicted by the 22 Hz seismic data coherence attribute. However, neither dataset was effective in detailing the fault zones).

(Yu et al., 2013), thus improving the continuity of fault identification based on coherence. Additionally, it effectively identifies subtle stratigraphic features that may be overlooked in full-bandwidth data (Alvarez San Román and Yutsis, 2019).

(2) The fault azimuth volume (FAV), which accurately reflects the planar distribution and cross-sectional characteristics of strike-slip faults in the study area, was obtained using intermediate data produced by an automatic fault extraction (AFE) process (Dorn et al., 2012). This volume was extracted using the AFE process from a commercial package provided by the Emerson Paradigm Company. The strike-slip fault distribution on the top surface of the Yingshan Formation in the study area was characterized using a combination of slicing and seismic profile interpretation.

(3) Segmentation of strike-slip faults involves dividing a single strike-slip fault into several independent units and then analyzing the structural characteristics of each segment (de Joussineau and Aydin, 2010). The vertical separations of various profiles on the top surface of the Yingshan Formation (T_7^4) were measured. The confirmation of fault step polarity and kinematics has been facilitated by observing alterations in the sign of vertical separations—positive indicating contractional deformation and negative indicating extensional deformation—documented along the fault strike, along with

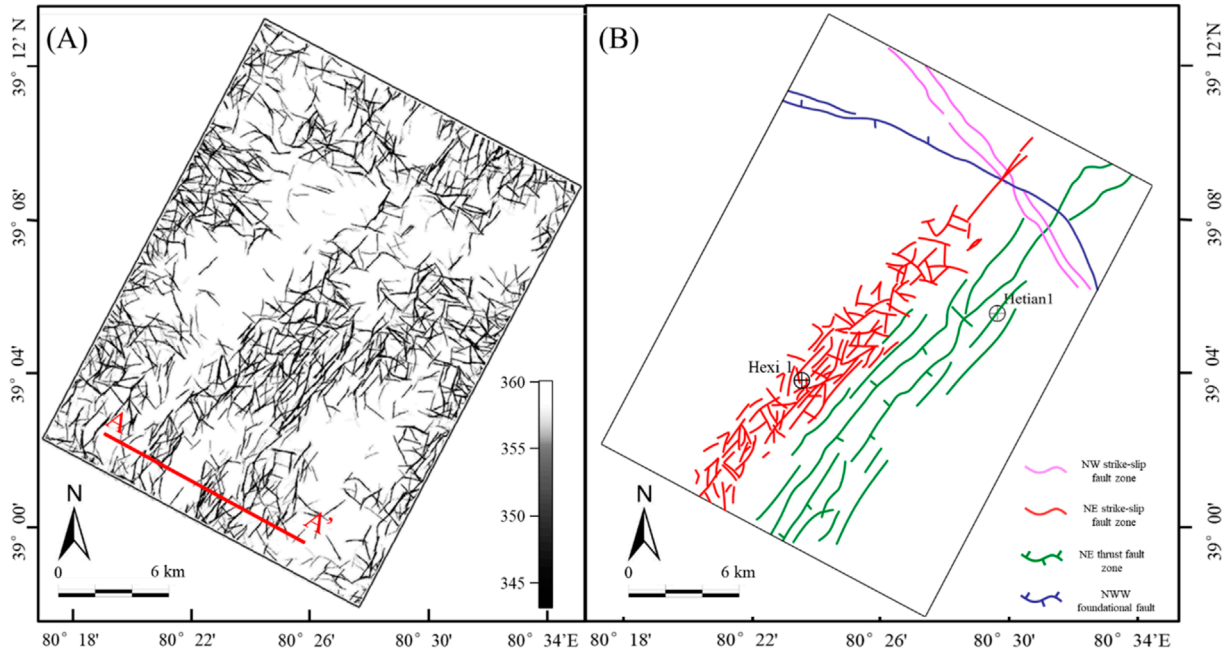

FIGURE 8
(A) Fault azimuth volume map of T_7^4. **(B)** Distribution map of faults in the study area. (AA' in the figure represents the profile location in Figure 9).

the corresponding magnitudes (Aydin and Nur, 1985; Biddle and Christie-Blick, 1985). The principles for segmenting strike-slip faults were based on these numerical values and a combination of structural and planar patterns in the fault profiles. Therefore, a comprehensive analysis of the segmented characteristics of strike-slip faults in the study area was conducted. A developmental model for the strike-slip fault zone in the eastern segment of the Bachu Uplift was established.

(4) The seismic attribute referred to as "Parallel Bedding Indicator (PBI)" is defined as the variance of the attribute "Dip-of-maximum similarity". The attribute represents the standard deviation of the instantaneous dips computed over the user-defined average dip computation window. Zones with parallel bedding will therefore show close to zero variance values (Riedel et al., 2012; Riedel et al., 2013). In fact, in this study, seismic amplitude was directly used as input. Areas with lower amplitude displayed smaller variance, thereby highlighting the 'strong amplitude string beads' features characteristic of fault-karst reservoirs in carbonate rocks (Wang et al., 2021).

These reservoirs are geologically anomalous bodies relative to the surrounding continuous carbonate formations. Consequently, during the propagation of seismic waves, these anomalous bodies interact with the surrounding rocks, creating strong wave impedance reflection interfaces. This results in a concentration of various energy waves, including reflection and diffraction waves, forming a strong energy group within a local area. This leads to typical "bright spot" reflections characterized by strong reflection amplitudes, long longitudinal extensions, and poor lateral continuity. This attribute was extracted using a parallel bedding indicator process from the commercial SKUA package from the Emerson Paradigm Company.

4 Results

4.1 Strike-slip fault zone characterization

Spectral decomposition preprocessing based on CWT was applied to the seismic data. From the amplitude spectrum (Figure 5), the frequency band range of the decomposed data volume remained within the effective frequency band of the original seismic data. Compared with the original seismic data (Figure 6A), the 22 Hz frequency-subdivided data volume (Figure 6B) exhibited the same fault segment characteristics along the base of the strike-slip fault zone (T_8^2) (indicated by yellow arrows); however, the flower structural features of the strike-slip fault zone at the top of the Yingshan Formation (T_7^4) (indicated by red arrows) were more pronounced. Therefore, it can be concluded that the 22 Hz frequency-subdivided data volume preserves the basic shape of the original structural features as well as highlights the details of the strike-slip fault zone.

Third-generation coherence technology was applied to calculate the coherency of the original and 22 Hz frequency-subdivided data. Extracting the plan view of the coherency volume along T_7^4 and comparing it with the coherency volume of the original data (Figure 7A), the coherency volume of the 22 Hz frequency-subdivided data reflected the position of the strike-slip fault zone (indicated by red arrows in Figure 7B). From the sections, the 22 Hz data (Figure 7D) volume provided a clearer and higher-resolution characterization of the strike-slip fault zone

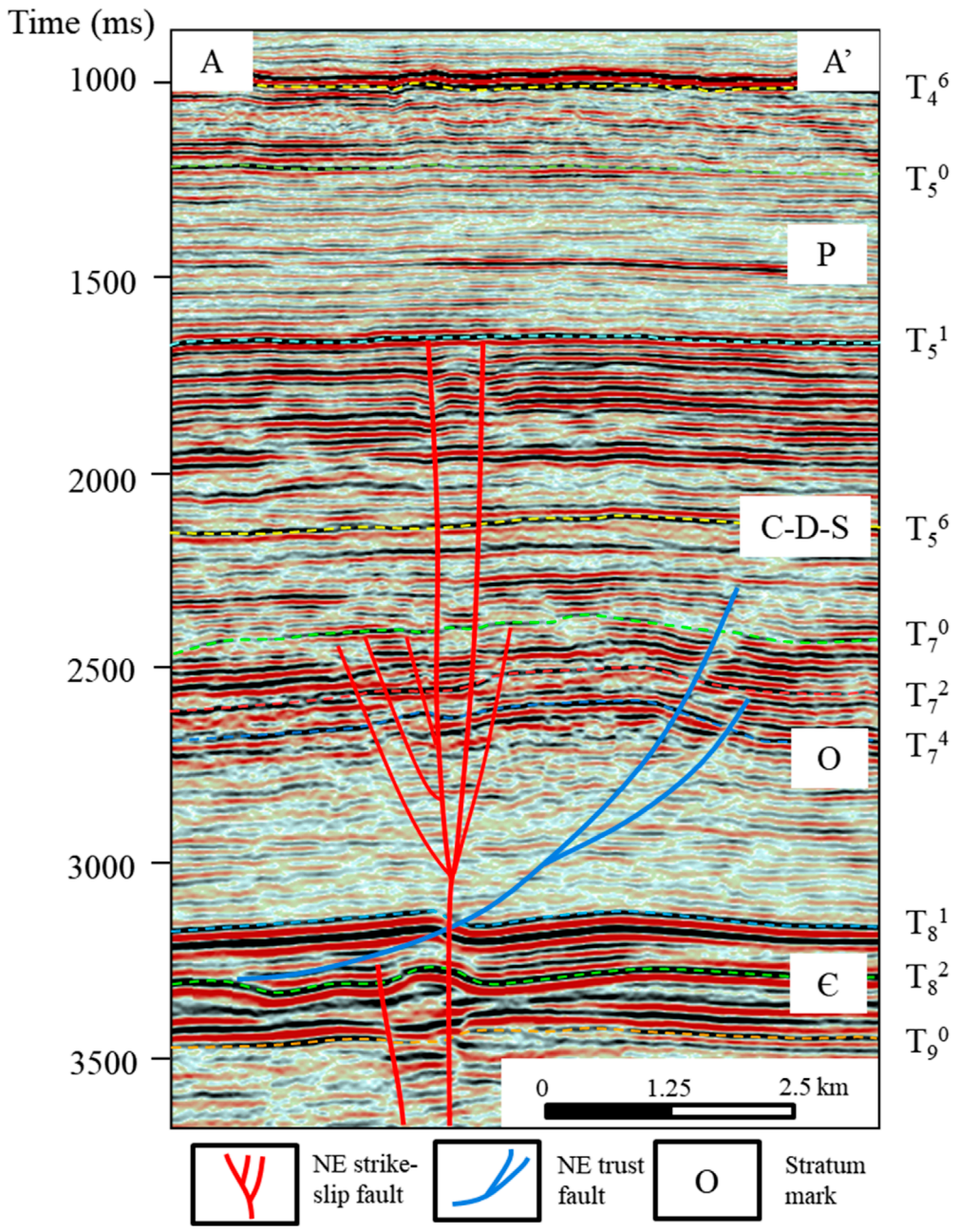

FIGURE 9
Northeast-trending strike-slip fault interpretation profile (profile location shown in Figure 8. The strike-slip fault cuts into the basement downward and locally extends into the Neogene upwards. The fault displacement is relatively small on the profile, and clear folding is visible at the top of the Permian and in the Middle and Lower Cambrian strata, with consistent vertical positions).

than raw data (Figure 7C). However, neither dataset was effective in detailing fault zones.

Figure 8A shows a FAV slice of the T_7^4 top of the Yingshan Formation (T_7^4) in the study area. This image shows the interpreted results for the fault network in the study area. The FAV accurately identified all faults in the study area and showed the details of the strike-slip fault zone. This meets the requirements for interpreting the segmentation features and development patterns of faults. The study area consists of four fault zones: a northwest foundational fault zone, northwest strike-slip fault zone, northeast thrust fault zone, and northeast strike-slip fault zone. The directions such as northwest and northeast indicate the strike orientation of the faults.

For a detailed interpretation, this study focused on the northeast strike-slip fault zone (highlighted in red in Figure 8B). The northeast-trending strike-slip fault zone cuts into the basement downward and locally extends into the Neogene upwards. The fault displacement is relatively small on the profile, and clear folding is visible at the top of the Permian and in the Middle

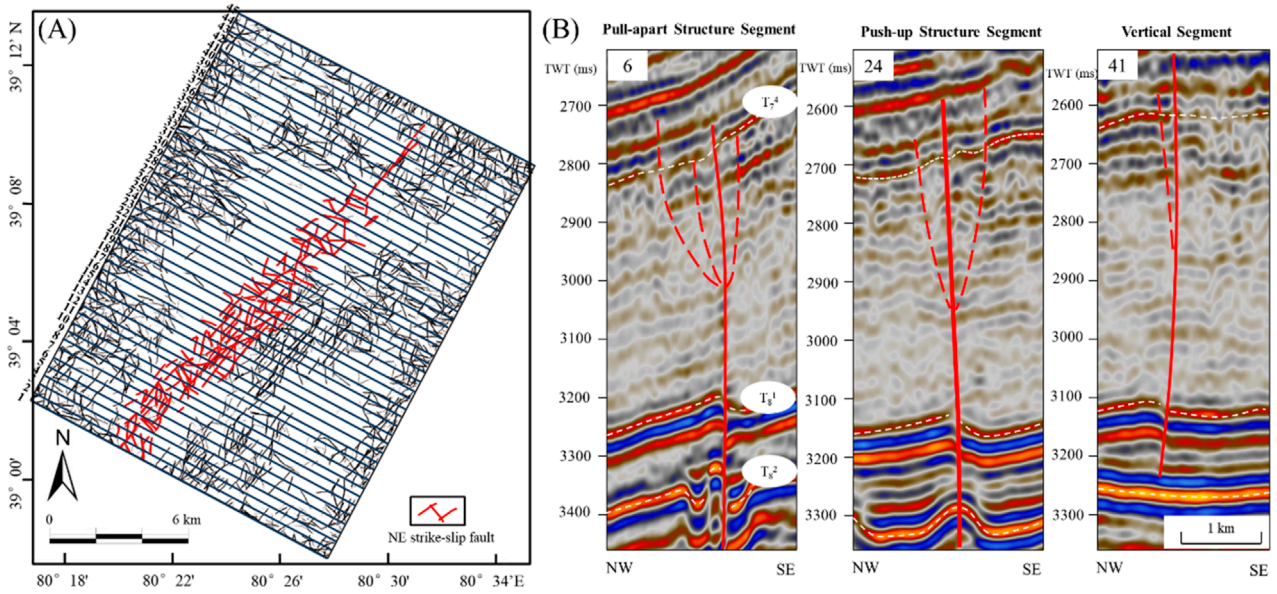

FIGURE 10
(A) FAV map of T_7^4. **(B)** The profile division of the northeast-trending strike-slip fault zone. (Fault interpretation of profiles 6, 24, and 41, which are perpendicular to the strike-slip fault zone. The main faults are indicated by bold red lines, and the branch faults are shown by thin red dashed lines).

and Lower Cambrian strata, with consistent vertical positions (Figure 9). This is similar to the strike-slip fault patterns observed in Shunbei (Sun et al., 2021; Yuan et al., 2021), confirming it as a strike-slip fault.

4.2 Segmenting the strike-slip fault zone

The Yingshan Formation (T_7^4) strike-slip fault zone in the study area exhibited varying vertical displacements, structural patterns, and planar configurations along its length. Vertical fault displacement across the T_7^4 was measured on each profile (Figure 10A), with positive values indicating contractional deformation and negative values indicating extensional deformation. Based on the profile characteristics of the strike-slip faults (Figure 10B), the northeast-trending strike-slip fault zone can be divided into three deformation segments: vertical, pull-apart, and push-up. Based on these three types of deformation segments, the northeast-trending strike-slip fault zone is subdivided into four segments in the 3D region: I and III are pull-apart segments, II is a push-up segment, and IV is a vertical segment (Figure 11).

In cross-sections, strike-slip faults are commonly observed as nearly vertical faults and exhibit flower structures. These flower structures represent a particular type of structure within the strike-slip fault systems. A positive flower structure was formed under a transpressional stress regime and appeared as a convex structure. In contrast, a negative flower structure was created in a transtensional stress field and took the form of a concave structure or could even evolve into a pull-apart basin on a larger scale. Both the positive and negative flower structures lacked fold geometrics. Nearly vertical fault-related structures were relatively straightforward, with the fault appearing nearly vertical in the cross-section, and the strata on either side of the fault exhibited lateral displacement. Strike-slip faults showed various planar configurations, including linear, horsetail splays, subparallel en echelons, and irregular geometrics in the horizontal view (Figure 12).

The cross-section of the vertical segment exhibited a high-angle, subvertical-linear structure (see Figure 12 vertical segment). The internal structure within the fault zone remained relatively constant, with limited development of secondary faults. There was a noticeable offset of the seismic waves on either side of the fault, with considerable displacement in the deeper parts than in the shallower sections. The planar configuration was relatively simple. At the tail end of this strike-slip fault segment, a horsetail splay with a relatively small branching angle was observed. In the push-up segment (see Figure 12 push-up segment), the cross-section exhibited the characteristics of a positive flower structure. The internal structure is complex and features multiple sets of branch faults that develop around the main fault. These branch faults had asymmetric sizes and shapes. The planar configuration was more intricate, including subparallel en echelon patterns formed by several branching faults and irregular geometrical shapes. For the pull-apart segment (see Figure 12 pull-apart segment), the cross-section showed a negative flower structure. The internal structure was similarly complex with the development of secondary faults. The predominant planar configuration included quadrilateral shapes; at the overlapping areas, it was approximated as a pull-apart type graben.

Different segments of the northeast-trending strike-slip fault zone in the study area exhibit distinct stress states and causative mechanisms. The mechanical origins of strike-slip faults can be classified into two main types: pure- and simple shear models (Sylvester, 1988). Many of the world's major strike-slip faults are classified in the category of simple shear, extending thousands of

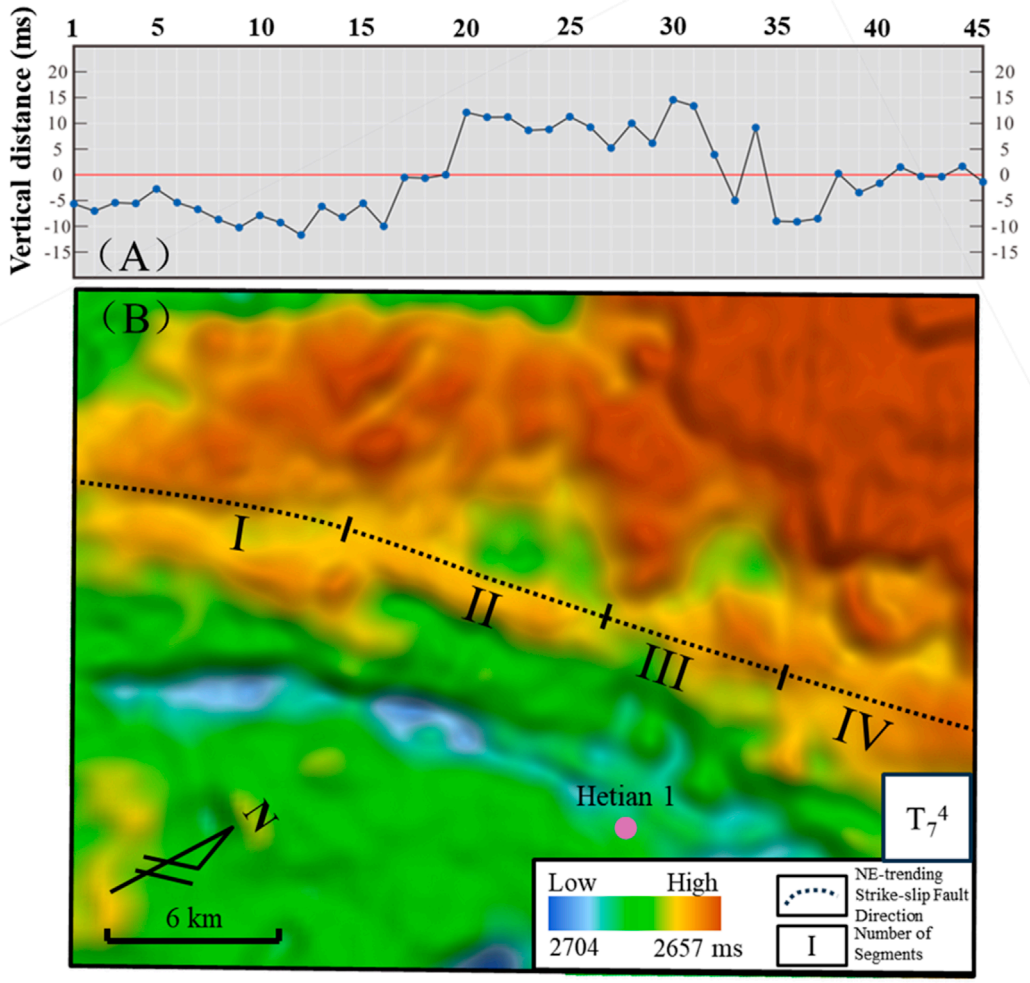

FIGURE 11
(A) Vertical fault displacement across T_7^4 of the northeast-trending strike-slip fault zone. **(B)** 3D topography of T_7^4 and segmentation features of the strike-slip fault zone in the study area. (I and III are pull-apart segments, II is a push-up segment, and IV is a vertical segment).

kilometers in length and tens of kilometers in width. Numerous laboratory experiments have confirmed the role of Riedel shearing in strike-slip fault systems (Naylor et al., 1986). The structural characteristics of the northeast-trending strike-slip fault zone in the study area conform to the Riedel shear model (Sylvester, 1988). Different combinations of fractures were developed in the vertical, push-up, and pull-apart segments (Figure 13). In the vertical segment, Y- and R-shear fractures were present. The push-up segment exhibited Y-, R-, P-, and R′-shear fractures. The pull-apart segment featured Y-, R-, P-, and R′-shear fractures. A detailed interpretation of strike-slip faults and a thorough analysis of fault details are crucial for subsequent development (Li et al., 2018).

The Ordovician strike-slip fault systems of the Tarim Basin are characterized as small-displacement strike-slip faults within stable craton interiors (Ma et al., 2019). In the Bachu Uplift, concealed basement faults are oriented in a near-northeast direction. Weak structural zones may develop in areas where these basement faults develop. Therefore, it can be inferred that the northeast-trending strike-slip fault zone in the study area was controlled by simple shear stress and formed within a pre-existing weak structural zone.

4.3 Reservoir characterization

Figure 14 shows core photographs from neighboring wells in the study area. These core sections were all within the Yingshan Formation. The core photograph from the Batan4 well (Figure 14A) revealed the development of a horizontal fracture reservoir. In the case of well He 4 (Figure 14B), the core photograph revealed the presence of dissolution cavity reservoirs with varying degrees of infill. The core sa mples from the Yubei8 well (Figures 14C, D) indicated that the reservoir primarily consisted of interconnected small dissolution pores. The core images from the He6 well (Figures 14E, F) showed a reservoir type characterized by fractures and interconnected dissolution pores. Although no core data were available for the Yingshan Formation in Hetian 1, the imaging logging data (Figures 14G–I) implied the existence of filled or unfilled dissolution pores and fractures in this formation. The eastern segment of the Bachu Uplift in the southwestern Tarim Basin primarily contains fault-karst reservoirs in the Yingshan Formation (Ji et al., 2012; Liu et al., 2018).

10.3389/feart.2024.1464924

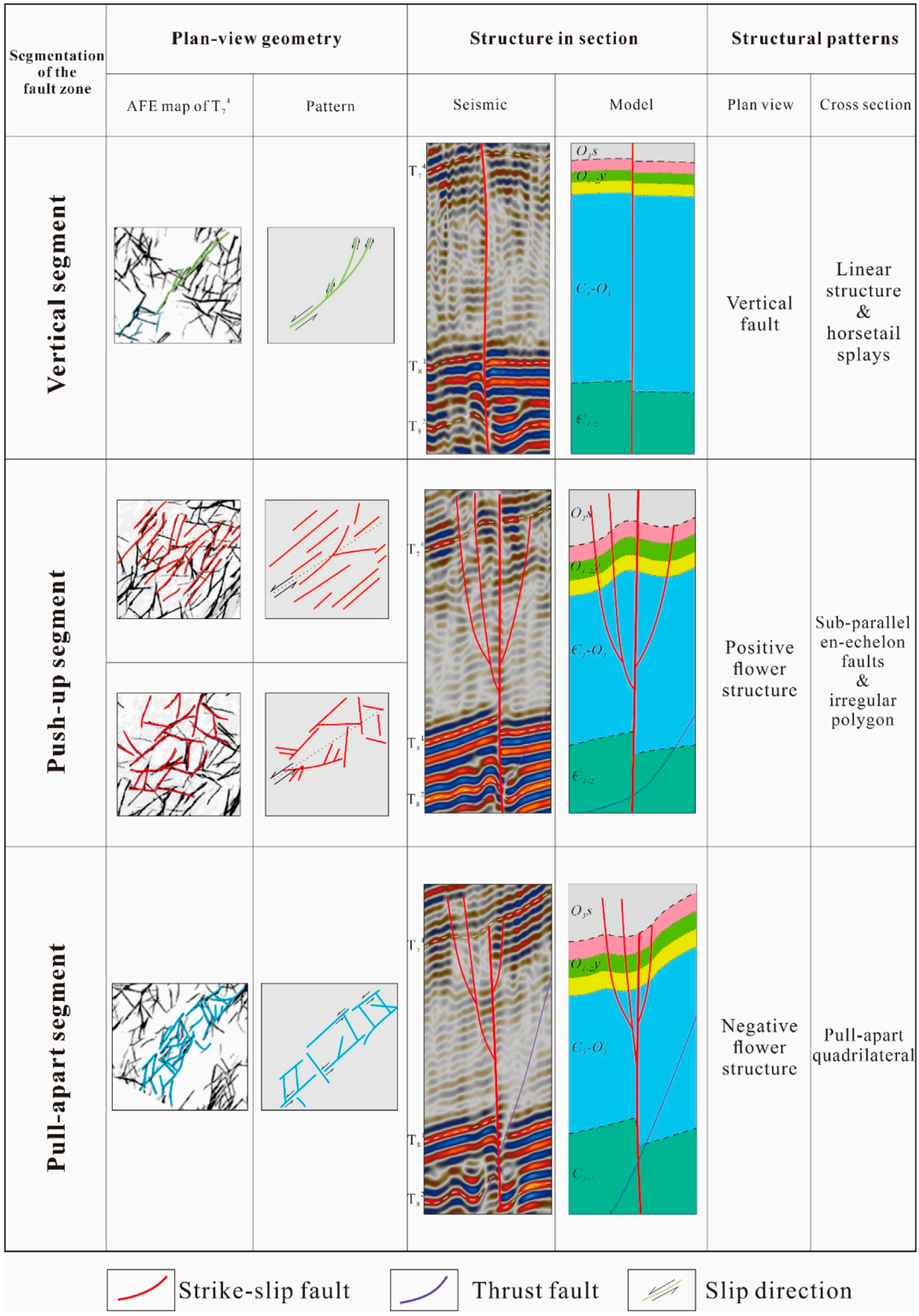

FIGURE 12
Structural styles of the NE strike-slip fault zone in the study area.

According to previous studies (Wang et al., 2021), fault-karst reservoirs typically exhibit low density (DEN), high acoustic (AC), and low P-impedance on well logs. In the study area, these reservoirs also show similar logging responses (Figure 15). The reservoir prediction results indicate that the PBI attribute closely matches the imaging logging data from HeTian1 well.

Segmentation of the fault zone	Fault azimuth volume map of T_7^4	Rose diagram	Riedel shears model	Description
Vertical segment	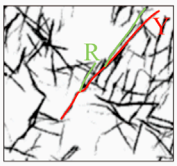	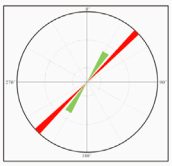	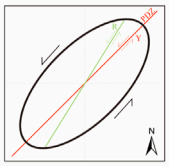	There are fewer secondary faults and the strike of the faults is more concentrated.
Push-up segment	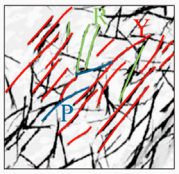	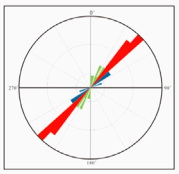	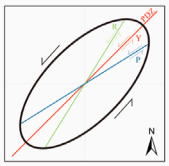	This segment mainly develops Y shears strike-slip faults, with a small amount of R shears and P shears strike-slip faults developed.
	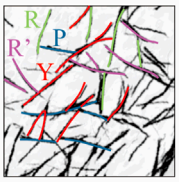	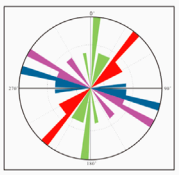	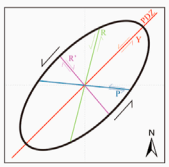	This segment can almost be explained by a complete Riedel shears model, which includes the development of Y shears, R shears, P shears, and R 'shears strike-slip faults.
Pull-apart segment		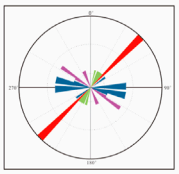	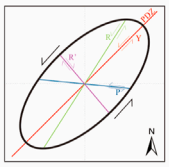	This segment can almost be explained by a complete Riedel shears model, with Y shears strike-slip faults having the longest length.
	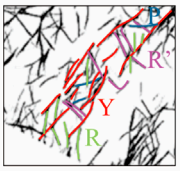		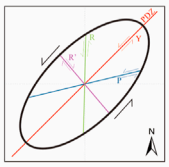	This segment can almost be explained by a complete Riedel shears model, with P shears strike-slip faults are less developed.

FIGURE 13
Faults combinations in different segments of the NE strike-slip fault zone.

Figure 16 shows the superposition of the Ordovician Yingshan Formation faults and fault-karst reservoirs in the study area. The results indicate that the reservoirs are primarily distributed along the fault zones with different reservoir development characteristics along various segments of the northeast-trending strike-slip fault zone. Reservoirs are less developed in the vertical segment, whereas the push-up and pull-apart segments are concentrated, exhibit more developed fractures. These fractures provide pathways for migrating fluids and increase the contact area between the fluids and the original rock, which is favorable for the development of fault-karst reservoirs. Among these segments, the push-up segment shows a higher degree of branching fractures, making it the most developed section in terms of reservoir quality.

5 Discussion

5.1 Storage characteristics of the strike-slip fault zone

The superimposition of the strike-slip fault on the Ordovician carbonate rocks, which underwent Late Caledonian and Early-Hercynian karst alterations, is favorable for the development of effective fracture-pore-type reservoirs. In the Bachu-Maigaiti area, the Middle to Lower Ordovician formations generally experienced karstification during the Middle Caledonian III tectonic episode, providing favorable conditions for the early formation of extensive karst reservoirs (Qian, 2014). Additionally, strike-slip faults can enhance the connectivity and effectiveness of these reservoirs (Zhang et al., 2021).

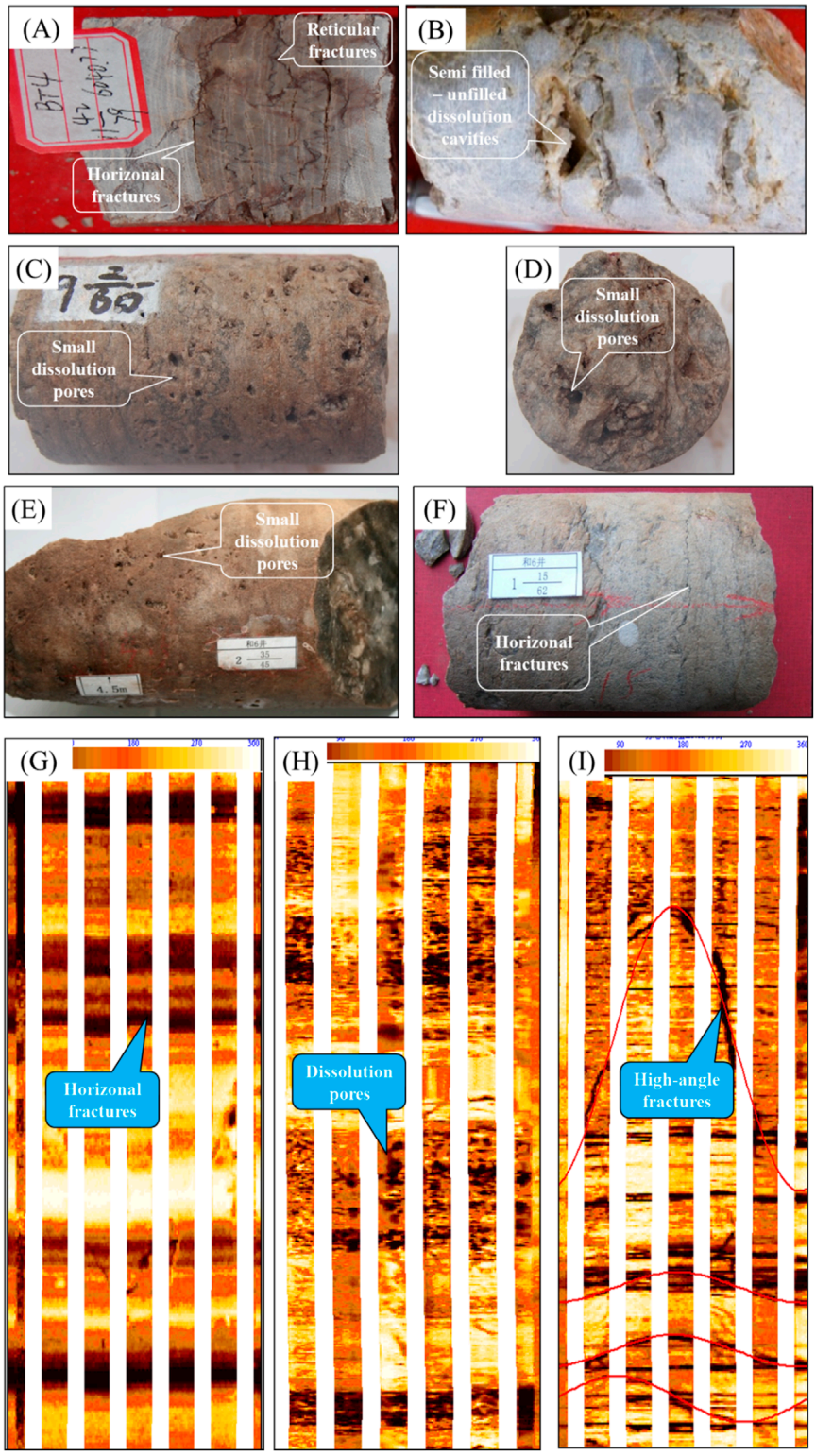

FIGURE 14
Core photos and dynamic enhanced EMI imaging logging data. **(A)**. Batan4 well, fractured reservoirs, 6,040.77 m, $O_{1\text{-}2}y$; **(B)**. He4 well, dissolved cavities reservoirs, $O_{1\text{-}2}y$; **(C)**. Yubei8 well, dissolved pores reservoirs, $O_{1\text{-}2}y$; **(D)**. Yubei8 well, cross-section photo of core, dissolved pores reservoirs, $O_{1\text{-}2}y$; **(E)**. He6 well, dissolved pores reservoirs, 3,195.74 m, $O_{1\text{-}2}y$; **(F)**. He6 well, fractured reservoirs, 3,768.28 m, $O_{1\text{-}2}y$; **(G)**. Hetian1 well, fractured reservoirs, 4,579–4,581 m, $O_{1\text{-}2}y$; **(H)**. Hetian1 well, dissolved pores reservoirs, 4,930–4,935 m, $O_{1\text{-}2}y$; **(I)**. Hetian1 well, fractured reservoirs, 4,939–4,943 m, $O_{1\text{-}2}y$).

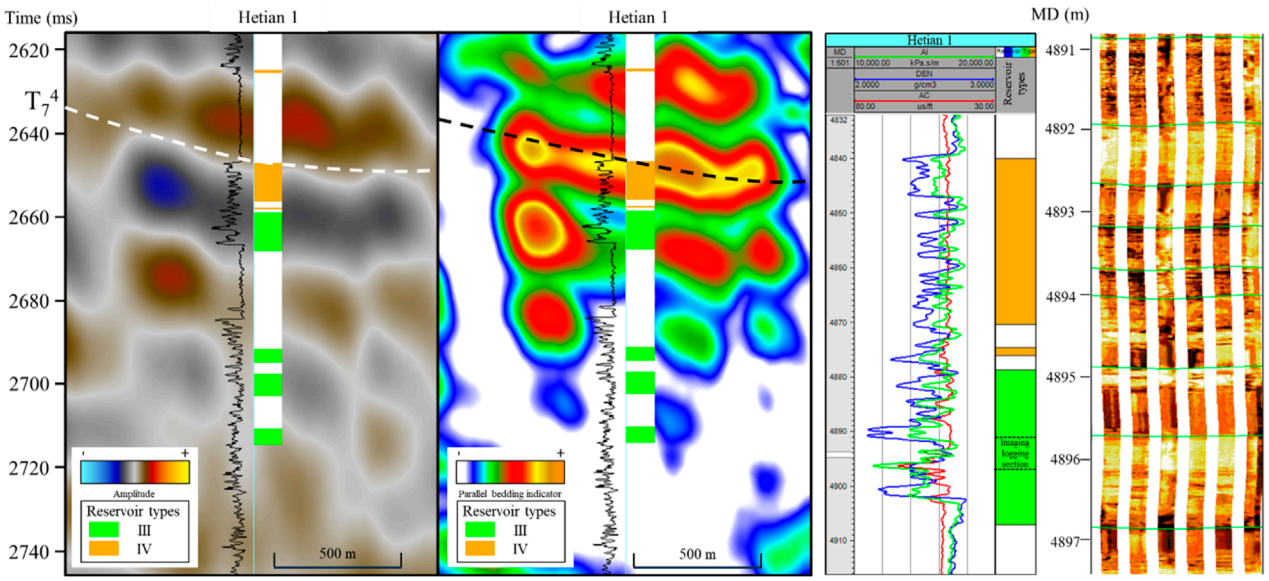

FIGURE 15
Comparison of the well-seismic combination. The prediction results of the PBI agree well with the reservoir drilled in HeTian1. The black curve in the profile represents the density log, and the dynamic imaging log data on the far right also shows dissolved pore reservoirs at 4,890–4,900 m).

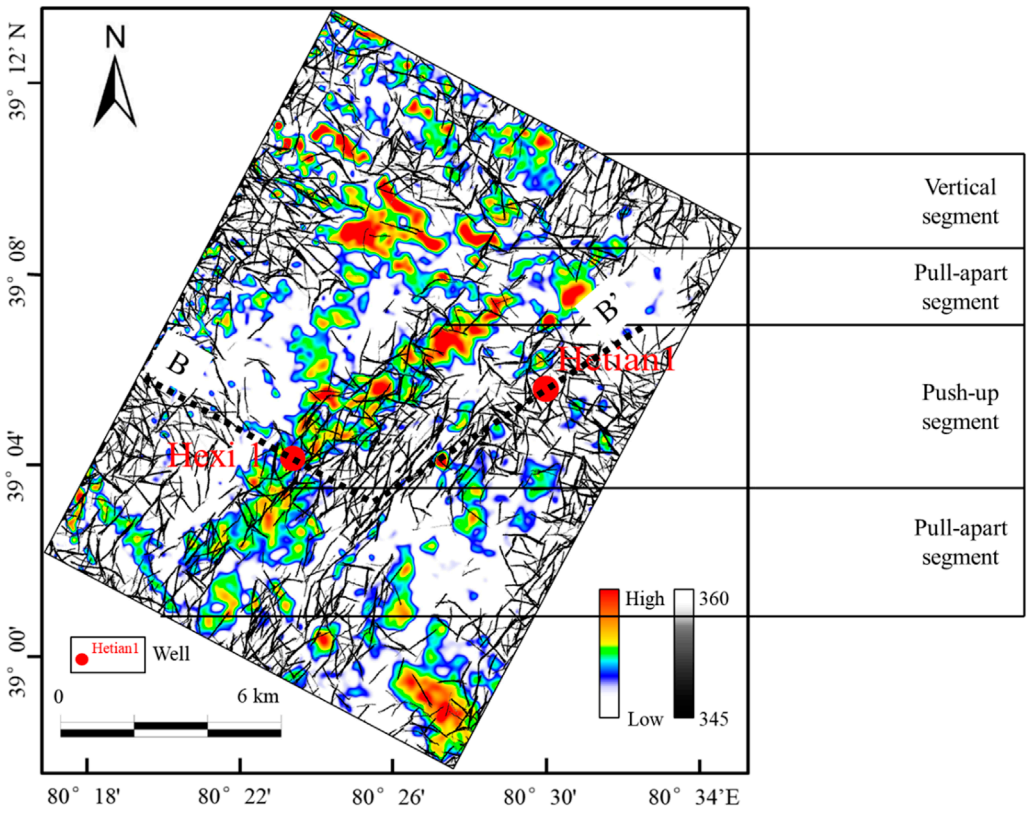

FIGURE 16
Superimposed map of parallel bedding indicator attribute and fault azimuth attribute in the study area (BB' in the figure represents the profile location in Figure 17).

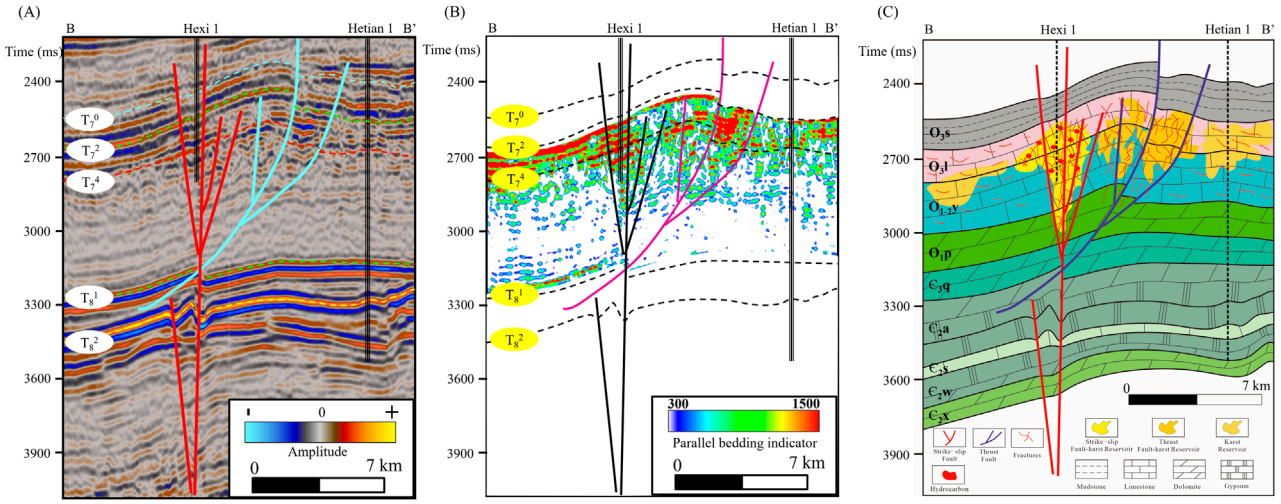

FIGURE 17
(A) Seismic profile; **(B)** Reservoir prediction results **(C)** Reservoir development model of HeXi1 well - HeTian1 well (profile location shown in Figure 15).

In the Tarim Basin, a series of normal faults developed during the Early Ordovician to Early Cambrian periods. Influenced by regional stress, these basement faults could evolve into high-angle strike-slip faults. The transformation of normal faults into strike-slip faults, forming flower structures, is a result of compressive stress, a phenomenon already demonstrated in Khan et al.'s research (Khan and Abdelmaksoud, 2020). The formation of the Bachu Uplift underwent four evolutionary stages. By the end of the Late Ordovician, the collision between the North Kunlun-Altyn block and the Tarim block led to the formation of a compressive contractional structural system (Bizhu et al., 2011), which is the tectonic deformation mechanism responsible for the formation of the strike-slip faults in the Bachu Uplift. During the same period, the salt layers above the Bachu Uplift's basement acted as a "lubricant," facilitating the formation of northeast-trending thrust faults (Khan et al., 2023). In subsequent stages, these faults continued to develop.

In the study area, the northeast-trending strike-slip fault zone and thrust fault zone develop together to form a northeast-trending fault system. This fault system is similar to the Yubei1 structural zone (Qiao et al., 2018), with strike-slip faults typically cutting downward into the Middle and Lower Cambrian strata or the basement, and upward through the salt layer into the crest of the anticline (Figure 17A) (Bian et al., 2022; Zhu et al., 2017). Some studies suggest that the oil and gas in the Bachu Uplift originate from the marine organic-rich mud shale beneath the salt in the southwestern Maigaiti slope (Cao et al., 2021; Ouyang et al., 2022; Zheng et al., 2022). Therefore, compared to the thrust fault above the Middle Cambrian salt, the strike-slip fault that cut through the salt directly to the basement are more conducive to guiding oil and gas to accumulate in the Ordovician formations (Figure 17C) (Zhang et al., 2023). Additionally, according to well data, HeXi one well in the study area first showed liquid hydrocarbon oil stains in the Bachu Uplift, while HeTian1 well showed no oil or gas shows. Based on this, it is suggested that the northeast-trending strike-slip fault zone is more favorable for hydrocarbon accumulation (Figure 17C).

Exploration has shown that oil-source faults, reservoir development, and local structural highs are the primary factors controlling hydrocarbon accumulation in the Ordovician strata of the Tarim Basin (Lu et al., 2017). Based on research into the segment characteristics of the strike-slip fault, reservoir development, the configuration of oil-source faults and branch faults, and local structural highs, a control and storage model for the Ordovician strike-slip fault in the study area was established (Figure 18). In the vertical segment (Figure 18A), fractured reservoirs are distributed along the fault in a strip-like pattern with relatively poor development, and oil and gas are not significantly enriched. In the push-up segment (Figure 18B), the main fault acts as an oil-source fault, while the branch fault serves as a lateral migration pathway for oil and gas and is a major control and storage fault. The reservoirs are mainly distributed on both sides of the branch fault, with the central high position being favorable for oil and gas accumulation and storage. In the pull-apart segment (Figure 18C), the main fault also serves as an oil source fault, and the reservoirs are distributed along the branch fault. The favorable accumulation area for oil and gas is located in the central high position, enclosed by R- and Y-shears. In this segment, oil and gas reservoirs are distributed at the edges of the fault zone. Hetian1 well has developed karst reservoirs associated with unconformities; however, it is located outside the fault zone, resulting in weak oil and gas charging and a lack of significant reserves. The oil and gas accumulation pattern of the Ordovician can be summarized as "hydrocarbon supply from external sources, fault-mediated migration, segmented reservoir control, and high-elevation accumulation."

5.2 Limitations of the study

The fault-karst reservoirs in the Tarim Basin exhibit strong heterogeneity, which is closely related to the strike-slip fault zones. Consequently, there is significant variation among these

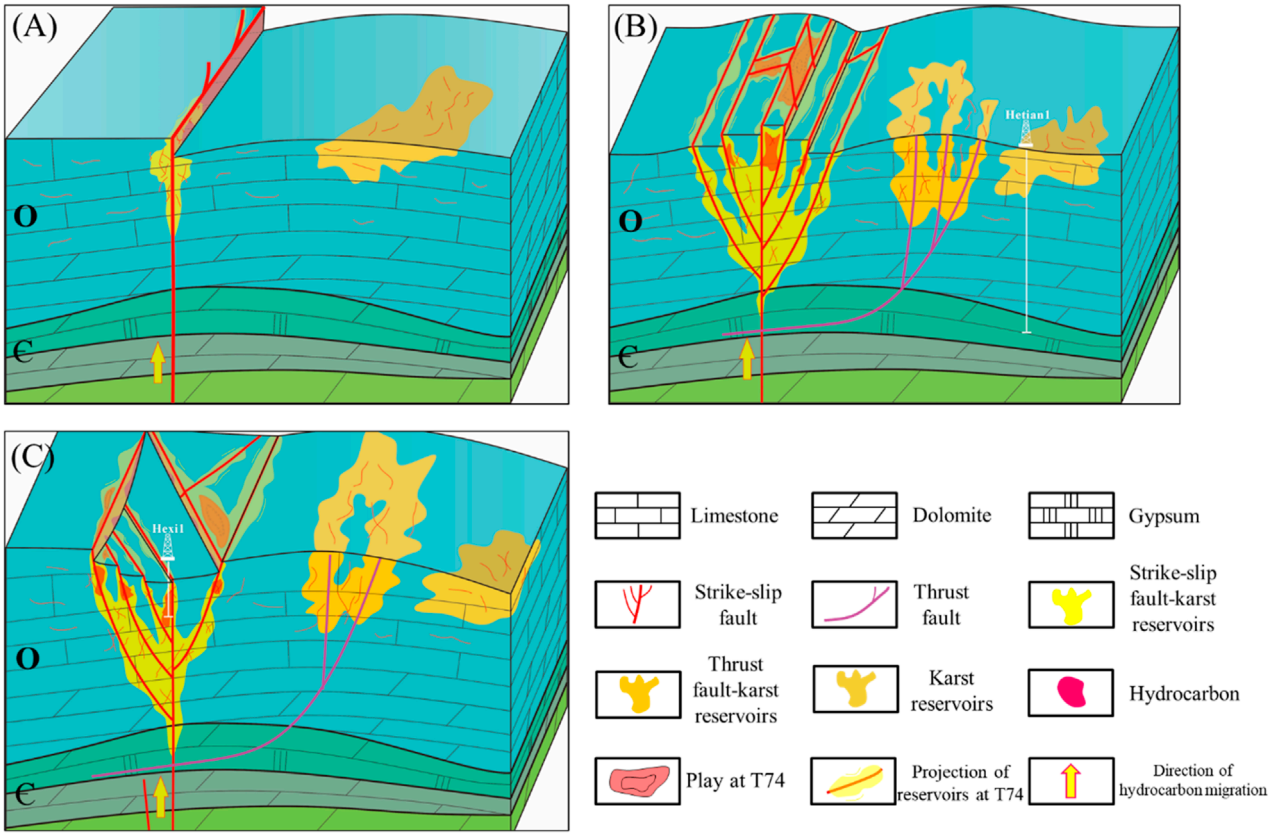

FIGURE 18
The control and storage model for the Ordovician strike-slip fault in the study area. (The strike-slip faults penetrating through the Cambrian and Ordovician strata in the figure are the main faults, while those developed only within the Ordovician are branch faults). **(A)** The vertical segment model. **(B)** The push-up segment model. **(C)** The pull-apart segment model.

reservoirs, making it challenging to effectively characterize their heterogeneity using the parallel bedding indicator attribute. However, this attribute proves valuable in describing these reservoirs. This study primarily emphasizes the influential role of strike-slip fault zones in controlling fault-karst reservoirs and potential hydrocarbon accumulation. The investigation does not address how branch faults contribute to the heterogeneity of these reservoirs. Future research will focus on collecting additional data, including more comprehensive well data from the study area, such as information on karst height and additional production data.

6 Conclusion

This study has demonstrated the significant value of seismic attributes in predicting and characterizing carbonate reservoirs. Specifically, seismic low-frequency information proved effective in identifying small displacement strike-slip faults, which serve not only as migration pathways but also as accumulation spaces for hydrocarbons. The parallel bedding indicator attribute was found to be a useful tool for describing the evolution of karst reservoirs.

The strike-slip faults in the southwestern Tarim Basin conform to the Riedel structural model, showing distinct segmentation in both cross-section and map views. Each segment exhibits unique characteristics and is associated with different hydrocarbon accumulation models. Based on these findings, an oil and gas enrichment model for the strike-slip fault zone was established, characterized by external hydrocarbon supply, fault-mediated migration, segmented reservoir control, and high-elevation accumulation. This model offers valuable insights for understanding the structural characteristics of strike-slip fault zones and guiding oil and gas exploration efforts in the southwestern Tarim Basin and other similar regions.

Data availability statement

The data analyzed in this study is subject to the following licenses/restrictions: The data that support the findings of this study are available from the corresponding author upon reasonable request. Requests to access these datasets should be directed to yrz@cumtb.edu.cn.

Author contributions

JG: Data curation, Project administration, Writing–original draft, Writing–review and editing. RY: Conceptualization, Methodology, Writing–review and editing. FG: Data curation, Resources, Writing–review and editing. LW: Conceptualization, Methodology, Project administration, Writing–original draft. SZ: Methodology, Software, Writing–review and editing. LnW: Formal Analysis, Writing–review and editing. FH: Methodology, Writing–review and editing.

Funding

The author(s) declare that financial support was received for the research, authorship, and/or publication of this article. This work was supported by the Fundamental Research Funds for the Central Universities (2022JCCXMT01).

Conflict of interest

Author FG was employed by Petroleum Exploration and Production Research Institute of Northwest Oilfield Company Sinopec.

The remaining authors declare that the research was conducted in the absence of any commercial or financial relationships that could be construed as a potential conflict of interest.

Publisher's note

All claims expressed in this article are solely those of the authors and do not necessarily represent those of their affiliated organizations, or those of the publisher, the editors and the reviewers. Any product that may be evaluated in this article, or claim that may be made by its manufacturer, is not guaranteed or endorsed by the publisher.

References

Alvarez San Román, F., and Yutsis, V. (2019). Application of spectral decomposition methods to the definition of stratigraphic features associated with channel reservoirs in the southeast petroleum province, méxico. *México Pure Appl. Geophys.* 176 (2), 873–883. doi:10.1007/s00024-018-1999-2

Aydin, A., and Nur, A. (1985). "The types and role of stepovers in strike-slip tectonics," in *Strike-slip deformation, basin formation, and sedimentation*. Editors K. T. Biddle, and N. Christie-Blick (SEPM Society for Sedimentary Geology), 37, 35–44. 0. doi:10.2110/pec.85.37.0035

Benesh, N. P., Plesch, A., and Shaw, J. H. (2014). Geometry, kinematics, and displacement characteristics of tear-fault systems: an example from the deep-water Niger Delta. *Aapg Bull.* 98 (3), 465–482. doi:10.1306/06251311013

Bian, Q., Deng, S., Lin, H., and Han, J. (2022). Strike-slip salt tectonics in the shuntuoguole low uplift, Tarim Basin, and the significance to petroleum exploration. *Mar. Petroleum Geol.* 139, 105600. doi:10.1016/j.marpetgeo.2022.105600

Biddle, K. T., and Christie-Blick, N. (1985). *Strike-slip deformation, basin formation, and sedimentation*. SEPM Society for Sedimentary Geology.

Bizhu, H., Cunli, J., Zhiqin, X., ZhiHui, C., ShiLin, L., and YingLi, Z. (2011). Manifestation of the Middle-Late Caledonian tectonic movement along the Altun-West Kunlun orogenic belt in the Tangguzibas depression, Tarim Basin. *Acta Perologica Sin.* 27 (11), 3435. doi:10.2110/jsr.2011.62

Brister, B. S., Stephens, W. C., and Norman, G. A. (2002). Structure, stratigraphy, and hydrocarbon system of a Pennsylvanian pull-apart basin in north-central Texas. *Aapg Bull.* 86 (1), 1–20. doi:10.1306/61eeda26-173e-11d7-8645000102c1865d

Cao, Z., Zhu, X., Wu, X., Xu, Q., Lu, Q., Li, J., et al. (2021). Source of hydrocarbons discovered from Cambrian sub-salt dolomite in Bachu Uplift area. *Tarim Basin Petroleum Geol. and Exp.* 43 (4), 648–654. doi:10.11781/sysydz202104648

Carne, R. C., and Little, T. A. (2012). Geometry and scale of fault segmentation and deformational bulging along an active oblique-slip fault (Wairarapa fault, New Zealand). *Bulletin* 124 (7-8), 1365–1381. doi:10.1130/b30535.1

Chemenda, A. I., Cavalie, O., Vergnolle, M., Bouissou, S., and Delouis, B. (2016). Numerical model of formation of a 3-D strike-slip fault system. *Comptes Rendus Geosci.* 348 (1), 61–69. doi:10.1016/j.crte.2015.09.008

Chen, J., He, D., Tian, F., Huang, C., Ma, D., and Zhang, W. (2022). Control of mechanical stratigraphy on the stratified style of strike-slip faults in the central Tarim Craton, NW China. *Tectonophysics* 830, 229307. doi:10.1016/j.tecto.2022.229307

Chopra, S., and Marfurt, K. (2007). Curvature attribute applications to 3D surface seismic data. *Lead. Edge* 26 (4), 404–414. doi:10.1190/1.2723201

Cui, L., Wu, K., Liu, Q., Wang, D., Guo, W., Liu, Y., et al. (2022). Enhanced interpretation of strike-slip faults using hybrid attributes: advanced insights into fault geometry and relationship with hydrocarbon accumulation in Jurassic formations of the Junggar Basin. *J. Petroleum Sci. Eng.* 208, 109630. doi:10.1016/j.petrol.2021.109630

de Joussineau, G., and Aydin, A. (2010). "Segmentation along strike-slip faults revisited," in *Mechanics, structure and evolution of fault zones*. Editors Y. Ben-Zion, and C. Sammis (Birkhäuser Basel), 1575–1594.

Deng, S., Li, H., Zhang, Z., Zhang, J., and Yang, X. (2019). Structural characterization of intracratonic strike-slip faults in the central Tarim Basin. *Aapg Bull.* 103 (1), 109–137. doi:10.1306/06071817354

Ding, W., Qi, L., Yun, L., Yu, T., Wu, L., Cao, Z., et al. (2012). The tectonic evolution and its controlling effects on the development of Ordovician reservoir in Bachu-Markit Tarim basin. *Acta Petrol. Sin.* 28 (8), 2542–2556. doi:10.3390/ijms141019618

Ding, W. L., Lin, C. S., Qi, L. X., Huang, T. Z., and Yu, T. X. (2008). Structural framework and evolution of Bachu uplift in Tarim basin. *Earth Sci. Front.* 15 (2), 242–252. doi:10.1016/S1872-5791(08)60056-1

Ding, Z. W., Wang, R. J., Chen, F. F., Yang, J. P., Zhu, Z. Q., Yang, Z. M., et al. (2020). Origin, hydrocarbon accumulation and oil-gas enrichment of fault-karst carbonate reservoirs: a case study of Ordovician carbonate reservoirs in South Tahe area of Halahatang oilfield, Tarim Basin. *Petroleum Explor. Dev.* 47 (2), 306–317. doi:10.1016/s1876-3804(20)60048-9

Dorn, G. A., Kadlec, B., and Murtha, P. (2012). Imaging faults in 3D seismic volumes. *Seg. Annu. Meet.*, 1538–2012.

Frankowicz, E., and McClay, K. R. (2010). Extensional fault segmentation and linkages, Bonaparte Basin, outer North west shelf, Australia. *Aapg Bull.* 94 (7), 977–1010. doi:10.1306/01051009120

Gui, B., He, D., Zhang, Y., Sun, Y., and Zhang, W. (2021). 3D geometry and kinematics of the niudong fault, baxian sag, bohai bay basin, eastern China—insights from high-resolution seismic data. *J. Struct. Geol.* 146, 104307. doi:10.1016/j.jsg.2021.104307

Han, X., Deng, S., Tang, L., and Cao, Z. (2017). Geometry, kinematics and displacement characteristics of strike-slip faults in the northern slope of Tazhong uplift in Tarim Basin: a study based on 3D seismic data. *Mar. Petroleum Geol.* 88, 410–427. doi:10.1016/j.marpetgeo.2017.08.033

He, B. Z., and Zheng, M. L. (2016). Structural characteristics and formation dynamics: a review of the main sedimentary basins in the continent of China. *Acta Geol. Sinica-English Ed.* 90 (4), 1156–1194. doi:10.1111/1755-6724.12766

He, G., He, Z., Zhang, H., Lin, L., Chen, Q., Qian, Y., et al. (2009). Paleozoic structural deformation of Bachu uplift, Tarim basin of Northwest China: implications for plate drifting. *J. Earth Sci.* 20, 755–762. doi:10.1007/s12583-009-0059-3

He, G., He, Z., Zhang, H., Zhu, Z., Chen, Q., Qian, Y., et al. (2007). Dual influence of the rejuvenation of southern tianshan and western Kunlun orogen on the cenozoic structure deformation of Tarim Basin, northwestern China: a superposition deformation model from Bachu uplift. *J. Zhejiang University-SCIENCE A* 8 (9), 1388–1394. doi:10.1631/jzus.2007.a1388

He, X., Tang, Q., Wu, G., Li, F., Tian, W., Luo, W., et al. (2023). Control of strike-slip faults on Sinian carbonate reservoirs in Anyue gasfield, Sichuan Basin, SW China. *Petroleum Explor. Dev.* 50 (6), 1282–1294. doi:10.1016/s1876-3804(24)60466-0

Ji, Y. G., Han, J. F., Zhang, Z. H., Wang, J. Y., Su, J., Wang, Y., et al. (2012). Formation and distribution of deep high quality reservoirs of ordovician yingshan Formation in the northern slope of the tazhong area in Tarim Basin. *Acta Geol. Sin.* 86 (7), 1163–1174. doi:10.3969/j.issn.0001-5717.2012.07.012

Jia, C., He, D., and Lu, J. M. (2004). Episodes and geodynamic setting of himalayan movement in China: oil and gas. *Geology* 25 (2), 121–125. doi:10.11743/ogg20040201

Jia, C., Ma, D., Yuan, J., Wei, G., Yang, M., Yan, L., et al. (2022). Structural characteristics, formation and evolution and genetic mechanisms of strizke–slip faults in the Tarim Basin. *Nat. Gas. Ind. B* 9 (1), 51–62. doi:10.1016/j.ngib.2021.08.017

Jia, C., and Wei, G. (2002). Structural characteristics and petroliferous features of Tarim Basin. *Chin. Sci. Bull.* 47, 1–11. doi:10.1007/bf02902812

Jia, C., Wei, G., and Wang, L. S. (1997). *The structural feature and Petroleum in Tarim Basin*. Beijing: China Petroleum Industry Press.

Kang, Y., and Kang, Z. (1996). Tectonic evolution and oil and gas of Tarim Basin. *J. Southeast Asian Earth Sci.* 3 (13), 317–325. doi:10.1016/0743-9547(96)00038-4

Khan, M., and Abdelmaksoud, A. (2020). Unfolding impacts of freaky tectonics on sedimentary sequences along passive margins: pioneer findings from western Indian continental margin (Offshore Indus Basin). *Mar. Petroleum Geol.* 119, 104499. doi:10.1016/j.marpetgeo.2020.104499

Khan, M., Nawaz, S., and Radwan, A. E. (2023). New insights into tectonic evolution and deformation mechanism of continental foreland fold-thrust belt. *J. Asian Earth Sci.* 245, 105556. doi:10.1016/j.jseaes.2023.105556

Kumar, P. C., Sain, K., and Omosanya, K. O. L. (2023). Geometry and Kinematics of strike-slip faults in the Dibrugarh field of the Upper Assam foreland basin, NE India. *Mar. Petroleum Geol.* 153, 106291. doi:10.1016/j.marpetgeo.2023.106291

Li, C., Wang, X., Li, B., and He, D. (2013). Paleozoic fault systems of the tazhong uplift, Tarim Basin, China. *Mar. Petroleum Geol.* 39 (1), 48–58. doi:10.1016/j.marpetgeo.2012.09.010

Li, J. Z., Tao, X. W., Bai, B., Huang, S. P., Jiang, Q. C., Zhao, Z. Y., et al. (2021). Geological conditions, reservoir evolution and favorable exploration directions of marine ultra-deep oil and gas in China. *Petroleum Explor. Dev.* 48 (1), 60–79. doi:10.1016/s1876-3804(21)60005-8

Li, M., Wu, G., Xia, B., Huang, T., Ni, B., Pang, S., et al. (2019). Controls on hydrocarbon accumulation in clastic reservoirs of the Tarim Craton, NW China. *Mar. Petroleum Geol.* 104, 423–437. doi:10.1016/j.marpetgeo.2019.04.008

Li, Q., Li, Y., Cheng, Y., Li, Q., Wang, F., Wei, J., et al. (2018a). Numerical simulation of fracture reorientation during hydraulic fracturing in perforated horizontal well in shale reservoirs. *Energy Sources, Part a Recovery, Util. Environ. Eff.* 40 (15), 1807–1813. doi:10.1080/15567036.2018.1486920

Li, W., Guo, W., Sun, S., Yang, X., Liu, S., and Hou, X. (2018b). Research on hydrocarbon accumulation periods of palaeozoic reservoirs in bachu–maigaiti area of Tarim Basin. *J. Jilin Univ. Earth Sci. Ed.* 48 (3), 56–67. doi:10.13278/j.cnki.jjuese.20170003

Li, Y., Ding, W., Zeng, T., Xia, W., Cheng, X., Shi, S., et al. (2023). Structural geometry and kinematics of a strike-slip fault zone in an intracontinental thrust system: a case study of the No. 15 fault zone in the Fuling area, eastern Sichuan Basin, southwest China. *J. Asian Earth Sci.* 242, 105512. doi:10.1016/j.jseaes.2022.105512

Liang, Y., Zhang, Y., Chen, S., Guo, Z., and Tang, W. (2020). Controls of a strike-slip fault system on the tectonic inversion of the Mahu depression at the northwestern margin of the Junggar Basin, NW China. *J. Asian Earth Sci.* 198, 104229. doi:10.1016/j.jseaes.2020.104229

Lin, C., Li, S., Liu, J., Qian, Y., Luo, H., Chen, J., et al. (2011). Tectonic framework and paleogeographic evolution of the Tarim basin during the Paleozoic major evolutionary stages. *Acta Petrol. Sin.* 27 (1), 210–218. doi:10.1134/S0024490211010007

Liu, H., Liu, B., and Cao, J. (2018). Characteristics and controlling factors of lower-middle Ordovician reservoirs in Yubei area. *Tarim Basin Oil and Gas Geol.* 39 (1), 107–118. doi:10.11743/ogg20180111

Lu, X., Wang, Y., Tian, F., Li, X., Yang, D., Li, T., et al. (2017). New insights into the carbonate karstic fault system and reservoir formation in the Southern Tahe area of the Tarim Basin. *Mar. Petroleum Geol.* 86, 587–605. doi:10.1016/j.marpetgeo.2017.06.023

Lu, X. X., Wang, Y. F., and Zhang, Y. P. (2016). Strike-slip faults and their control on differential hydrocarbon enrichment in carbonate karst reservoirs: a case study of Yingshan Formation on northern slope of tazhong uplift, Tarim Basin. *Acta Geol. Sinica-English Ed.* 90 (2), 761–762. doi:10.1111/1755-6724.12708

Lv, Y., Ma, H., Wang, Z., Deng, G., and Wen, H. (2022). Genetic types of the tp12cx strike-slip fault segments and their role in controlling reservoirs in the Tarim Basin. *Front. Earth Sci.* 10. doi:10.3389/feart.2022.916475

Ma, D., Wu, G., and Zhu, Y. (2019). Segmentation characteristics of deep strike slip faults in the Tarim Basin and its control on hydrocarbon enrichment: taking the Ordovician strike slip fault in the Halahatang Oilfield in the Tabei area as an example. *Earth Sci.* 26, 225–237. doi:10.13745/j.esf.sf.2019.1.10

Naylor, M. A., Mandl, G., and Supesteijn, C. H. K. (1986). Fault geometries in basement-induced wrench faulting under different initial stress states. *J. Struct. Geol.* 8 (7), 737–752. doi:10.1016/0191-8141(86)90022-2

Ouyang, S. Q., Lyu, X. X., Xue, N., Li, F., and Wang, R. (2022). Paleoenvironmental characteristics and source rock development model of the Early-Middle Cambrian: a case of the Keping-Bachu area in the Tarim Basin. *J. China Univ. Min. Technol.* 51 (2), 293–310.

Pang, X. Q., Tian, J., Pang, H., Xiang, C. F., Jiang, Z. X., and Li, S. M. (2010). Main progress and problems in research on Ordovician hydrocarbon accumulation in the Tarim Basin. *Petroleum Sci.* 7 (2), 147–163. doi:10.1007/s12182-010-0022-z

Qi, L. (2021). Structural characteristics and storage control function of the Shun I fault zone in the Shunbei region, Tarim Basin. *J. Petroleum Sci. Eng.* 203, 108653. doi:10.1016/j.petrol.2021.108653

Qian, Y. T. Z. L. (2014). Lithofacies, diagenesis zone and reservoir origin of the Ordovician in eastern tectonic belt of the Maigaiti slope. *Oil Gas Geol.* 35, 870–882. doi:10.11743/ogg20140614

Qiao, G., Zheng, H., Yu, T., Luo, Y., and Luo, S. (2018). Fault belt reservoir controls in Yubei area, Tarim Basin. *Petroleum Geol. and Exp.* 40 (5), 662–668.

Ramadhan, A., Samudra, A. B., Lestari, E. P., Saputro, J., Hirosiadi, Y., Amrullah, I., et al. (2018). strike-slip fault deformation and its control in hydrocarbon trapping in ketaling area, jambi subbasin, Indonesia. *Jambi Subbasin, Indonesia 41St Hagi Annu. Convention Exhib. 2016* 132, 012025. doi:10.1088/1755-1315/132/1/012025

Riedel, M., Bahk, J., Kim, H., Yoo, D., Kim, W., and Ryu, B. (2013). Seismic facies analyses as aid in regional gas hydrate assessments. Part-I: classification analyses. *Mar. Petroleum Geol.* 47, 248–268. doi:10.1016/j.marpetgeo.2013.04.011

Riedel, M., Bahk, J. J., Scholz, N. A., Ryu, B. J., Yoo, D. G., Kim, W., et al. (2012). Mass-transport deposits and gas hydrate occurrences in the Ulleung Basin, East Sea – Part 2: gas hydrate content and fracture-induced anisotropy. *Mar. Petroleum Geol.* 35 (1), 75–90. doi:10.1016/j.marpetgeo.2012.03.005

Rotevatn, A., and Bastesen, E. (2014). Fault linkage and damage zone architecture in tight carbonate rocks in the Suez Rift (Egypt): implications for permeability structure along segmented normal faults. *Geol. Soc. Lond. Spec. Publ.* 374 (1), 79–95. doi:10.1144/sp374.12

Shen, W., Chen, J., Wang, Y., Zhang, K., Chen, Z., Luo, G., et al. (2019). The origin, migration and accumulation of the Ordovician gas in the Tazhong III region, Tarim Basin, NW China. *Mar. Petroleum Geol.* 101, 55–77. doi:10.1016/j.marpetgeo.2018.11.031

Sinha, S., Routh, P. S., Anno, P. D., and Castagna, J. P. (2005). Spectral decomposition of seismic data with continuous-wavelet transform. *Geophysics* 70 (6), P19–P25. doi:10.1190/1.2127113

Song, Z., Tang, L., and Liu, C. (2021). Variations of thick-skinned deformation along tumuxiuke thrust in Bachu uplift of Tarim Basin, northwestern China. *J. Struct. Geol.* 144, 104277. doi:10.1016/j.jsg.2021.104277

Sun, Q., Fan, T., Gao, Z., Wu, J., Zhang, H., Jiang, Q., et al. (2021). New insights on the geometry and kinematics of the Shunbei 5 strike-slip fault in the central Tarim Basin, China. *J. Struct. Geol.* 150, 104400. doi:10.1016/j.jsg.2021.104400

Sun, Z., Yang, R., Geng, F., Wang, L., Wang, L., and Guo, J. (2023). Analyzing the formation and evolution of strike-slip faults and their controlling effects on hydrocarbon migration and charging: a case study of tahe area, Tarim Basin. *Tarim. Basin Energies* 16 (5), 2370. doi:10.3390/en16052370

Sylvester, A. G. (1988). Strike-slip faults. *Geol. Soc. Am. Bull.* 100 (11), 1666–1703. doi:10.1130/0016-7606(1988)100<1666:ssf>2.3.co;2

Tong, D., Zhang, J., Yang, H., Hu, D., and Ren, J. (2012). Fault system, deformation style and development mechanism of the Bachu uplift, Tarim basin. *J. Earth Sci.* 23 (4), 529–541. doi:10.1007/s12583-012-0273-2

Wang, B., Chen, C., Shang, J., Lei, M., Zhu, W., Qu, Y., et al. (2023). Characteristics and controlling role in hydrocarbon accumulation of strike-slip faults in the Maigaiti slope. *Processes* 11 (4), 1049. doi:10.3390/pr11041049

Wang, L., Yang, R., Li, D., Meng, L., and Xiao, Z. (2021). Seismic attributes for characterization and prediction of carbonate faulted karst reservoirs in the Tarim Basin, China: interpretation-a. *J. Subsurf. Charact.* 9 (3), T611–T622. doi:10.1190/int-2019-0162.1

Wang, Z., Gao, Z., Fan, T., Shang, Y., Qi, L., and Yun, L. (2020). Structural characterization and hydrocarbon prediction for the SB5M strike-slip fault zone in the Shuntuo Low Uplift, Tarim Basin. *Mar. Petroleum Geol.* 117, 104418. doi:10.1016/j.marpetgeo.2020.104418

Woodcock, N. H., and Fischer, M. (1986). Strike-slip duplexes. *J. Struct. Geol.* 8 (7), 725–735. doi:10.1016/0191-8141(86)90021-0

Wu, G., Ma, B., Han, J., Guan, B., Chen, X., Yang, P., et al. (2021). Origin and growth mechanisms of strike-slip faults in the central Tarim cratonic basin, NW China. *Petroleum Explor. Dev.* 48 (3), 595–607. doi:10.1016/s1876-3804(21)60048-4

Wu, G., Yang, H., He, S., Cao, S., Liu, X., and Jing, B. (2016). Effects of structural segmentation and faulting on carbonate reservoir properties: a case study from the Central Uplift of the Tarim Basin, China. *Mar. Petroleum Geol.* 71, 183–197. doi:10.1016/j.marpetgeo.2015.12.008

Xiang, X., Chen, L., Lu, S., Yan, Z., and Tang, J., (2023). Mantle plume impingement and lithosphere rejuvenation: a case of Tarim craton: progress in Geophysics, 38, no. 1, 86–100.

Xiao, Y., Wu, G. H., Lei, Y. L., and Chen, T. T. (2017). Analogue modeling of through-going process and development pattern of strike-slip fault zone. *Petroleum Explor. Dev.* 44 (3), 368–376. doi:10.1016/s1876-3804(17)30043-5

Yao, Y., Zeng, L., Dong, S., Huang, C., Cao, D., Mao, Z., et al. (2024). Using seismic methods to detect connectivity of fracture networks controlled by strike-slip faults in ultra-deep carbonate reservoirs: a case study in northern tarim basin, China. *J. Struct. Geol.* 180, 105060. doi:10.1016/j.jsg.2024.105060

You, X., Wu, S., and Xu, F. (2018). The characteristics and main control factors of hydrocarbon accumulation of ultra-deep marine carbonates in the tarim basin, nw China - a review. *Carpathian J. Earth Environ. Sci.* 13 (1), 135–146. doi:10.26471/cjees/2018/013/013

Yu, H., Li, J., Zhang, Y., and Xu, G., (2013). Research and application of spectral decomposition in carbonate reservoir and fault identification in MaiJie let gas field , *Amu Darya Basin Sustain. Dev. Nat. Resour.*, Pts 1-3, 616–618. doi:10.4028/www.scientific.net/AMR.616-618.141

Yu, J. B., Zhang, J., and Shi, B. P. (2010). A study on tectono-thermal evolution history of Bachu uplift in Tarim basin. *Chin. J. Geophysics-Chinese Ed.* 53 (10), 2396–2404. doi:10.1002/cjg2.1550

Yuan, H., Chen, S., Neng, Y., Zhao, H., Xu, S., Wang, X., et al. (2021). Composite strike-slip deformation belts and their control on oil and gas reservoirs: a case study of the northern part of the Shunbei 5 strike-slip deformation belt in Tarim Basin, Northwestern China. *Front. Earth Sci.* 9, 755050. doi:10.3389/feart.2021.755050

Zhang, Z., Kang, Y., Lin, H., Han, J., Zhao, R., Zhu, X., et al. (2021). A study on the reservoir controlling characteristics and mechanism of the strike slip faults in the northern slope of Tazhong uplift, Tarim Basin, China. *Arabian J. Geosciences* 14 (8), 735. doi:10.1007/s12517-021-07076-5

Zhang, Z., Xu, Q., Liu, S., Zhou, Y., Qiu, H., Lu, H., et al. (2023). Characteristics of NE strike-slip fault system in the eastern section of Bachu-Maigaiti area, Tarim Basin and its oil-gas geological significance. *Petroleum Geol. and Exp.* 45 (4), 761.

Zhao, R., Kang, Y., Han, J., Zhu, X., Zhao, T., Liu, Y., et al. (2023). Study on of structural style of fault zone and reservoir characteristics in the northern slope of Tazhong Uplift, Tarim Basin, China. *Carbonates Evaporites* 38 (2), 41. doi:10.1007/s13146-023-00851-3

Zheng, J., Li, B., and Yuan, Q. (2022). Hydrocarbon accumulation process and exploration direction of the deep Cambrian in Bachu-Tabei area. *Tarim Basin Oil and Gas Geol.* 43 (1), 79–91.

Zhu, X. J., Chen, J. F., He, L. W., Wang, Y. F., Zhang, W., Zhang, B. S., et al. (2017). Geochemical characteristics and source correlation of hydrocarbons in the well luosi 2 of Maigaiti slope, Tarim Basin, China. *Nat. Gas. Geosci.* 28 (4), 566–574. doi:10.11764/j.issn.1672-1926.2017.03.001